UNIVERSITÀ DEGLI STUDI DI PADOVA

DIPARTIMENTO DI INGEGNERIA INDUSTRIALE
CORSO DI LAUREA MAGISTRALE IN MATERIALS ENGINEERING

Tesi di Laurea Magistrale in
Materials Engineering

Carbon fiber/SiOC ceramic matrix composite truss-based structures fabricated via UV-assisted robot direct ink writing

Supervisor: Prof. Giorgia Franchin
Co-supervisor: Dott. Anna De Marzi

Candidate: Nicole Sturaro

ANNO ACCADEMICO 2023-2024

Abstract

Ceramic matrix composites (CMCs) are composites that contain inorganic fibers with ceramics as the matrix. The ceramic substrate in CMCs helps maintain the use of ceramics under load at very high temperatures (i.e., > 1000 °C) and improves the toughness and reliability of ceramics, particularly overcoming their intrinsic brittleness. Traditional manufacturing techniques for CMCs involve liquid- or gas-phase infiltration of carbon or ceramic fiber preforms with a precursor, followed by thermal cross-linking in an autoclave and pyrolysis. However, such manufacturing processes make it difficult, expensive, and time consuming to obtain complex-shaped CMCs that meet the requirements of engineering applications such as in aerospace (i.e., in turbine blades, heat shields), transportation (i.e., brake discs, engine components), and armor (i.e., ballistic protection panels, body armor).

In this sense, additive manufacturing (AM) techniques represent the best solution: thanks to their layer-by-layer process and the selective deposition of material, AM allow the fabrication of custom and complex geometries, thus avoiding the use of expensive molds and/or the need of post-machining steps. On the other hand, conventional AM techniques, such as Direct Ink Writing (DIW) and vat photopolymerization, are limited in the fabrication of CMCs due to the poor control on the fibers orientation and the need of support and/or sacrificial materials for the fabrication of fine features or severe overhangs. Furthermore, AM technologies are based on layer-by-layer approach, generating in this way interfaces, thus leading to lower strength and mechanical response of the printed structures.

From such perspective, the best approach is represented by the combination of two or more AM technologies into a unique hybrid technique. UV-assisted DIW (UV-DIW), for example, is based on the extrusion of a photo-curable suspension through a nozzle which is consequently cured enabling retention of its shape in thin air, thus avowing the use of supports and allowing the fabrication of support-less features. As a further step forward in overcoming the limitations of traditional AM, UV-DIW has been proven able to be coupled with a 6-axis robot arm; in this way, it is possible not only to increase the degree of freedom of the printable structures but especially to orient the printing head in the direction of the extruded filament, thus selectively align the fibers. This is particularly advantageous in the fabrication of strut-based lattice structures which are characterized by a regular pin-jointed frame made of trusses and surrounded by a void space. Thanks to their connectivity, such

structures can distribute the stresses and to create a rigid and un-foldable geometry with a strength-to-weight ratio suitable for lightweight applications.

This thesis project explored the fabrication and mechanical enhancement of lightweight, truss-based structures using UV-assisted Direct Ink Writing (UV-DIW) technology coupled with a 6-axis robot arm. The research activity focused on the preparation of a silicon-based photocurable ink reinforced with chopped carbon fibers, achieving a final fiber volume of 20%. The suspension needs to maintain adequate fluidity under shear force to ensure smooth delivery to the print point and exhibit good UV light reactivity, despite the black color of the carbon fibers, which does not reflect UV light. The pre-ceramic matrix contained an organic component, which was eliminated during the sintering process. The presence of the fibers caused constrained matrix shrinkage and crack formation during pyrolysis. To address this, different steps of pre-ceramic polymer infiltration and pyrolysis were performed to compensate for these cracks and ensure structural integrity. A analysis of the flexural strength was performed.

Index

Index of tables

Index of figures

Chapter 1
Introduction

In this chapter, general information about the principles of this thesis are given as well as the motivation of the proposal. Also, general organization of this thesis will be described.

1.1 Framework

Ceramic matrix composites (CMCs) consist of a ceramic-based matrix reinforced with ceramic particles, whiskers, or fibers. This unique association of materials makes CMCs able to withstand extreme environmental conditions, such as high temperature and corrosive atmosphere. CMCs, compared to traditional structural materials, exhibit higher thermal resistance and enhanced mechanical properties, due to their fibers-reinforced structure. Thanks to the synergic action of their constituents (i.e., matrix and reinforcement), such materials can be used in high performance applications, where thermal stability, high mechanical strength, and resistance to aggressive environments are required [1]. Moreover, they are widely used in structural applications as an alternative to metal alloys due to their higher strength-to-weight ratio and fracture toughness. Indeed, thanks to the introduction of secondary phases, the brittle nature of the ceramic matrix is hindered: the presence of reinforcing fibers creates controlled interfaces that interrupt crack propagation, preventing catastrophic failures. One typical feature of CMCs is the weak interface adhesion between matrix and fibers, which is developed using a thin interface layer. This design filament allows fiber sliding where microcracks initiate in the matrix, leading to more prudent battle against catastrophic failures and better damage tolerance.

Conventional CMCs manufacturing techniques, which include Chemical Vapor Infiltration (CVI) as well as Polymer Infiltration and Pyrolysis (PIP), are based on the impregnation of fiber preforms with matrix precursors. CVI involves the diffusion of gaseous precursors into a porous fiber preform where they react to form a solid ceramic matrix through chemical deposition on the fiber surfaces. PIP relies on repeated cycles of vacuum infiltration with liquid preceramic polymers followed by thermal

treatments to convert them into ceramic phases. While effective, such methods are prone to leave behind several defects in terms of residual porosities and cracks, thus requiring for the optimization of multiple infiltration steps. Moreover, they are limited in terms of geometrical complexity as they rely on the manufacturing of a mold, and consequently resulting in complex, expensive and time-consuming processes.

From these perspectives, the use of Addictive Manufacturing (AM) technologies represents an exciting solution to overcome such restrictions: due to their layer-by-layer process and the selective deposition of material, AM allow the fabrication of custom and complex geometries, thus avoiding the use of expensive molds and/or the need of post-machining steps [2]. Especially UV-assisted Direct Ink Writing (UV-DIW) enables the realization of complex structures without the need for support materials, while also improving fibers orientation using 6-axis robotic arm.

1.2 Objectives

The aim of this thesis is the fabrication of truss-based short carbon reinforced silicon oxycarbide (SiOC) matrix composites with the UV-assisted Direct Ink Writing (UV-DIW) technology. Such material and process combination are set to further expand the field of research for both CMCs and AM. Indeed, the enhanced freedom of design offered by UV-DIW is expected to enable the custom orientation of the reinforcement along the truss axes and thus maximize the mechanical response of the overall structure.

Additionally, this study aims to analyze the mechanical behavior of the prints truss structures, with particular focus on flexural strength.

1.3 Thesis Organization

This thesis is organized into chapters, each explaining a key aspect of the research.

- Chapter 1 provides a general introduction to the topic, states the motivations behind the study, and outlines the experimental approach that will be followed.

- Chapter 2 reviews the state of art in this field, discussing existing research and identifying the aspect that still need improvement.
- Chapter 3 describes the experimental procedures, describing the materials, methods, and equipment used during this study.
- Chapter 4 presents the experimental results and provides a discussion of the findings.
- Chapter 5 summarizes the conclusion of that thesis

Chapter 2

State of Art

This Chapter presents an overview about the state of art on this field of research, including the main issues related to the traditional CMCs manufacturing techniques, as well as how AM technologies can overcome their limitations and the relevance of lattice-based structures in the fabrication of components for structural applications.

2.1 Preceramic polymers

Preceramic polymers (PCPs) represent a class of polymeric materials which, through controlled thermal treatment, can be converted into ceramics. This class of materials distinguish itself by combining work versatility with the excellent thermal and mechanical properties of the ceramic materials [3] [4].

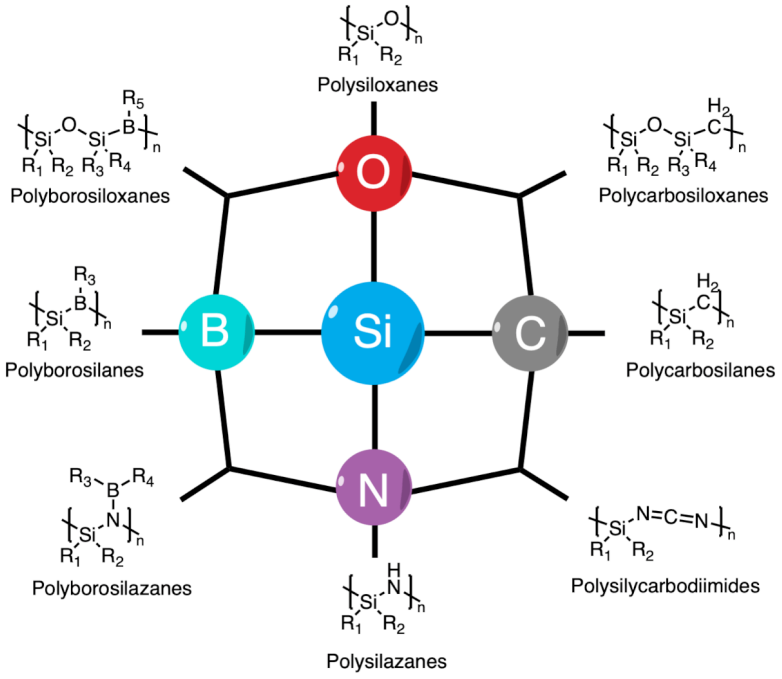

Figure 2.1. Common examples of preceramic polymer families.

The fundamental characteristic of PCPs is their molecular structure, which is typically a silicon-based backbone with various elements (C, O, N, B) in the principal or side chain. PCPs can be classified into different categories based on their chemical structures and backbone composition. The principal classes are: polysilanes (for SiC synthesis), polycarbosilanes (to produce SiC), polysilazanes (for Si_3N_4 or SiCN synthesis), polysiloxanes (to produce SiOC) and polysilsesquioxanes (used for complex SiOC structure) [5] [6] [7].

The use of preceramic polymers to produce ceramic components presents several advantages compared to traditional methods based on ceramics powders. First, thanks to their liquid state, PCPs can be processed using typical forming techniques used for polymers, such as injection molding, extrusion, resin transfer molding, and melt spinning, or dispersed in organic solvents to obtain inks for additive manufacturing (AM) (see §2.4) [7]. In addition to that, the conversion from polymer to ceramic happens at significantly lower temperatures (800-1200°C) compared to those required for sintering ceramic powders (>1300°C), with consequent energy savings [8]. Moreover, it is possible to tailor the molecular structure of preceramic polymers and thus obtain ceramics with homogeneous and optimized compositions. These compositions are not affected by the densification mechanisms of particles, mostly driven by the diffusion ability of atoms at the grain boundaries, which is a challenge in the case of ceramics powders [9].

2.2 Ceramics Matrix Composites

Traditional ceramic materials, despite presenting excellent properties such as high thermal resistance, oxidation resistance and chemical stability, are characterized by low toughness that limits their application features [10]. Ceramics Matrix Composites (CMCs) were developed to overcome that limitation, combining the advantageous properties of ceramics with the higher fracture resistance and cracks propagation [10] [11]. In recent years, there was a remarkable interest in research and development of wide variety of advance CMCs [10]. These materials find applications in thermal structures, exhaust nozzles, turbo pump discs, combustor linings, heat exchangers, and other applications that involve severe service condition. The fundamental characteristic of CMCs is the presence of the reinforcement fibers within the ceramic matrix, which provide higher mechanical resistance and higher strength compared to the traditional monolithic ceramics [11].

Despite their properties, traditional manufacturing processes of CMCs such as Chemical Vapor Infiltration (CVI) and Polymer Infiltration and Pyrolysis (PIP), and Reactive Melt Infiltration (RMI), present several advantages and drawbacks. CVI, for instance, is considered the most used technology to produce CMCs [10]. This process consists of the infiltration of fibrous and porous preforms with gaseous precursors that reacts or decompose to form the ceramic matrix [10]. This technique includes several steps: 1) preparation of fibrous preform with the desired structure, 2) introduction of gaseous precursors in a reaction chamber, 3) diffusion of gaseous in the preform, 4) chemical reaction and deposition of ceramic material on the fibers, 5) repetition of the cycle until the desired densification is reached (Figure 2.2).

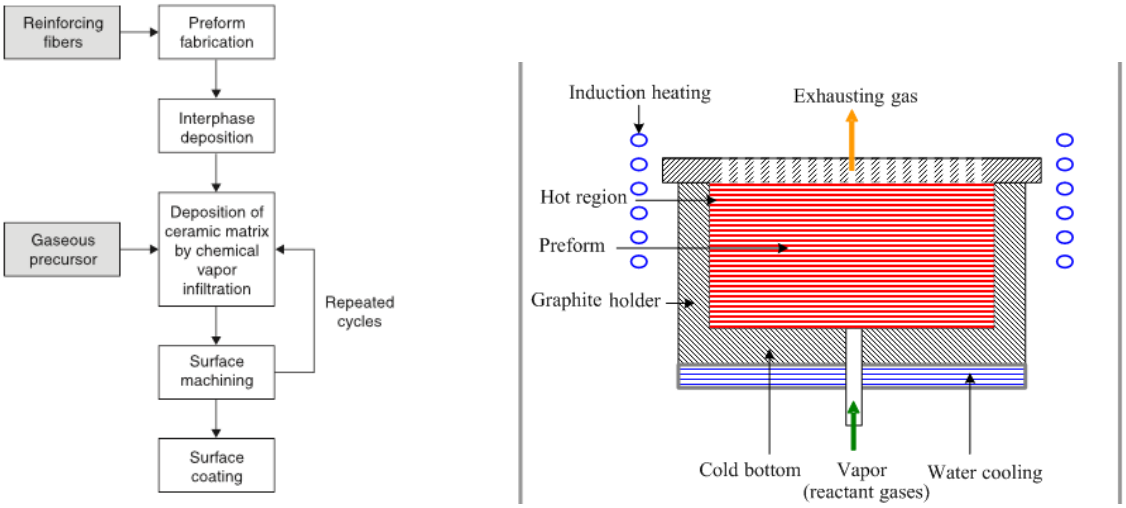

Figure 2.2. Fabrication of CMCs by CVI and graphical representation of the manufacturing process.

Despite it is the most common technique, CVI presents some significant disadvantages, such as the difficulty achieving uniform and complete densification of large components with complex geometries and the long process times [10]. Moreover, the facilities needed to process CMCs via CVI are expensive thus leading to high overall costs for the fabrication of parts.

On the other hand, PIP consists of the subsequent steps: 1) impregnation of fibrous preform with liquid polymeric precursor, 2) curing of the impregnated polymer, 3) conversion of the polymer into ceramic through pyrolysis at high temperature, 4) repetition of infiltration and pyrolysis cycles to improve the composite density [10] (Figure 2.3). While requiring for a much easier setup, PIP technique is prone to leave behind many closed porosities as usually the ceramic yield of the preceramic liquid is low, and it is difficult to fully coat and impregnate the fibers. By that, PIP usually

requires the repetition of multiple cycles of infiltration and pyrolysis, contributing significantly to increase components cost [10].

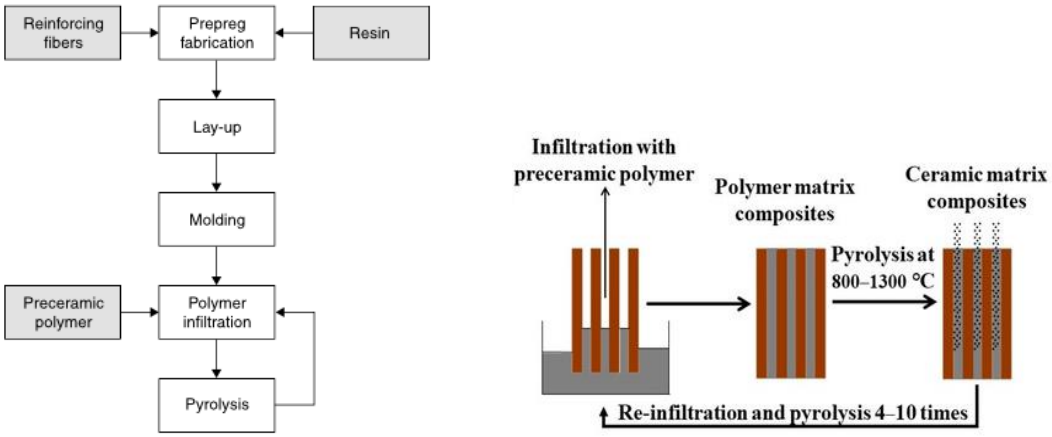

Figure 2.3. Fabrication of CMCs by PIP and graphical representation of the manufacturing process.

Compared to CVI and PIP, RMI is a cost- and time-efficient technique to produce ceramic matrix composites with low porosity. Indeed, the process is based on the introduction of a liquid molten metal into a preform through a pressure gradient caused by capillary action or by applied pressure. Since the chemical conversion to ceramic happens in situ between the melt and the preform, RMI is quick and efficient, requiring only hours to obtain the final CMC part (CVI instead can take up to a week to complete [12]). This approach allows to obtain highly dense composites in a single infiltration step but can lead to the formation of undesired phases and residual stresses due to the elevated process temperature and chemical reaction [10].

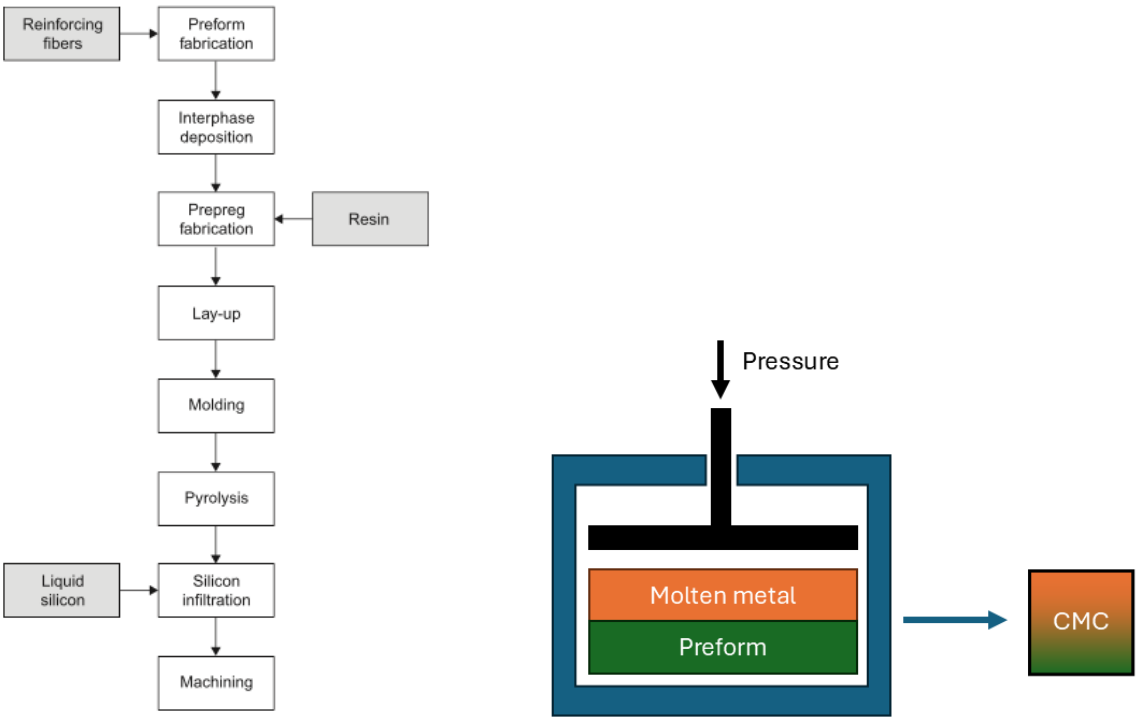

Figure 2.4. Fabrication of CMCs by RMI and graphical representation of the manufacturing process.

2.3 Structure and properties of composite materials

CMCs represent a category of composite called "inverse", in the sense that the deformation to fracture of the matrix is less compared to the fibers, that is the contrary of what happens in the case of polymeric or metallic matrix [13]. Thanks to this effect, CMCs exhibit a unique failure mode where the ceramic matrix may crack but the composite maintains its structural integrity thanks to the load-bearing capacity of the fibers, resulting in higher toughness and more predictable failure behavior compared to traditional monolithic ceramics.

Ceramic matrices can be oxides or non-oxides [14]. The first include materials like alumina (Al_2O_3), zirconia (ZrO_2) and silicon-based glass-ceramic. These matrices present excellent resistance in oxidizing environments but less creep resistance at high temperature. On the other hand, non-oxide matrices such as silicon carbide (SiC) and silicon nitride (Si_3N_4), offer high thermal stability, but are generally more sensible to oxidation [15]. The fibers commonly used includes both oxide (such as Al_2O_3 and mullite) and non-oxide (such as SiC) ceramic fibers [16]. The oxide fibers show high resistance to oxidizing environments, but limited strength resistance and creep resistance at high

temperature due to grain growth [13]. The non-oxide fibers, like carbon fibers, instead presents lower density and better strength resistance at high temperature. The fracture resistance of carbon fibers increases with temperature up to 150-200°C, while the SiC fibers maintain significant values resistance until 1400-1500°C [15].

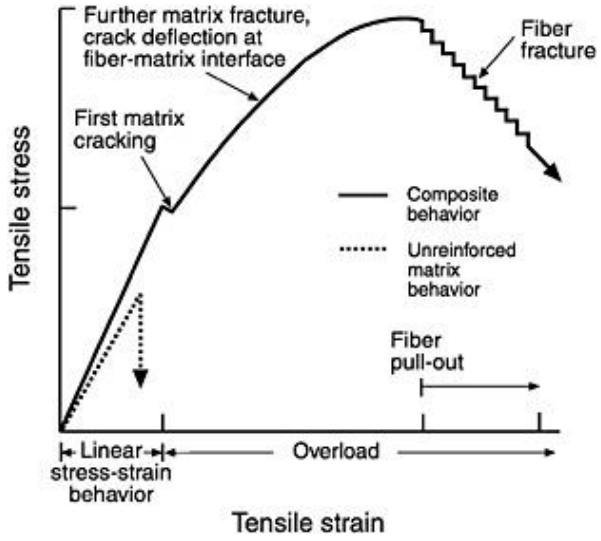

Figure 2.5. Effect of the reinforcement on the mechanical properties of a composite.

A fundamental aspect in the CMCs design is the control of the matrix/fiber interface as it play an important role in the mechanical behavior of these materials. Indeed, despite occupying a small volumetric fraction of the overall composite, the interface is responsible for transferring the stresses from the matrix to the fibers, deviating the cracks through fracture toughening mechanisms such as fiber bridging and fiber pullout [14] [16]. The key role of the reinforcement is to provide support to the brittle matrix, stopping crack propagation and preventing catastrophic failures (Figure 2.5). Compared to monolithic ceramics that are brittle, CMCs demonstrate higher resistance to crack propagation, thanks to the reinforcement mechanisms offered by the fibers [17]. The fracture in composite materials follows a specific mechanism: under load, the ceramic matrix fails like all ceramic materials upon elongation of 0.05%. In CMCs, however, the incorporated fibers act as bridges between the cracks [17]. This bridging mechanism is fundamental to guaranteeing higher stiffness and strength against the catastrophic failures typical of traditional ceramics. This higher resistance to failure of CMCs is effective only when the matrix can slide along the fibers, meaning there should be a weak bond between fibers and matrix.

2.4 Additive Manufacturing and new perspective for CMCs

Additive Manufacturing (AM) techniques represents an innovation in the production of ceramics and CMCs components. Such fabrication methods are based on the layer-by-layer material deposition guided by CAD models, eliminating the need for molds. In recent years, AM has focused on the CMCs production due to its ability to realize complex and customizable geometries which are difficult to achieve using the conventional technologies (see §2.2) [18]. The application of AM to CMCs has grown exponentially, with continuous improvement in both the process and materials. The ability to design and fabricate structures with optimized geometries, controlled distribution of the materials and specific functional properties represents a drastic shift compared to the traditional methods. [19]. AM offers many advantages for ceramic and CMC production. It provides high degree of freedom of design and enabling complex geometries that maximize component performance. The technology supports rapid prototyping capabilities, reducing time-to-market and development costs while eliminating the need for molds and reducing equipment costs. Additionally, AM facilitates the production of functionally gradient materials and multi-components in the same printing session, integrating structural and functional capabilities with lower fabrication time, reduced equipment needs, and decreased overall costs [20].

The AM techniques most used for CMCs includes Stereography (SLA), Selective Laser Sintering (LSL), and Direct Ink Writing (DIW). SLA was the first AM technology adopted for ceramic materials. The process is based on the photopolymerization of liquid resin containing suspended ceramic powders. Exposure to UV light polymerizes the resin, creating the desired geometry, in a layer-by-layer fashion. The components subsequently undergo thermal treatments to remove the binder and sinter the ceramic powders [21] [22]. Key advantages include high resolution and the capability to produce complex structural shapes, while the limitations concern the limitations maximum dimensions and the challenges in binder removal.

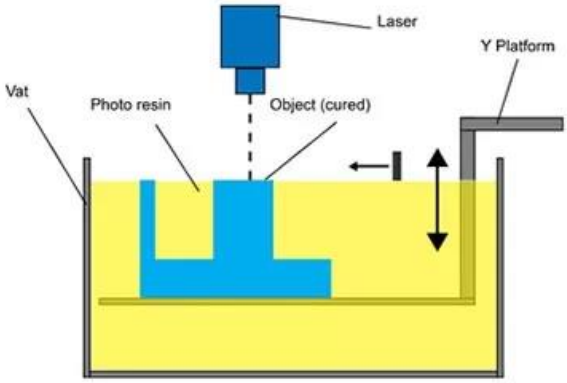

Figure 2.6. Schematic of Stereography (SLA)

On the other hand, the SLS employs a high-power laser to sinter or melt ceramic powders, building the desired component layer-by-layer. This technique presents different challenges caused by the high melting point and low thermal conductivity of the ceramic powders and can cause thermal stresses and cracks during the process [23]. Despite these disadvantages, recent research has demonstrated the possibility to obtain dense ceramic structures using innovative approaches such as pre-sintering, use of additives with low melting points or the use of preceramic polymers.

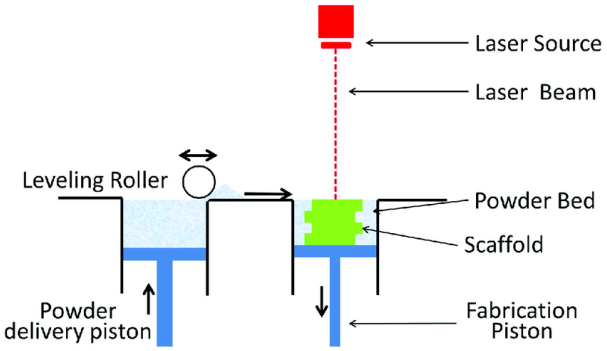

Figure 2.7. Schematic of Selective Laser Sintering (LSL)

The main disadvantages of SLA and SLS for producing CMCs are quite significant. SLA suffers from limited availability of ceramic-compatible photosensitive resins, severely restricting process versatility. SLS requires excessive energy for laser sintering, making it less economically viable. Both technologies demand expensive, complex equipment, substantially increasing production costs compared to the simpler [24] [23].

Compared to SLA and SLS, DIW is the most versatile method for the fabrication of advanced ceramics and CMCs. This technique involves extruding ink through a nozzle, allowing excellent control deposition of material along the printing trajectory to realize the desired structure [25]. DIW offers advantages, such as the possibility to use different ceramic materials and compositions, the capability to create complex structures and precise control of microstructure [26]. Specifically for CMCs, the advantage of DIW relies on its basic principle: the extrusion forces applied to the ink help in unidirectionally orienting the fiber reinforcement as it is squeezed and aligned in the direction of the filament [27]. This approach allows the design of materials with anisotropy properties, optimizing the mechanical response in specific directions based on the application requirements.

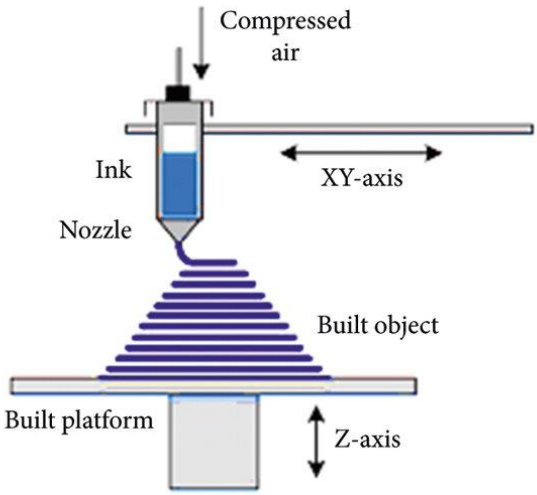

Figure 2.8. Schematic of Direct Ink Writing (DIW)

Despite its advantages, AM faces challenges that require further research and development. The surface quality and the dimensional precision are critical aspects, as 3D-printed ceramic components usually need post processing (i.e., machining or polishing) to achieve high surface finish. The densification represents another challenge, with the necessity to obtain components without defects or residual porosity. Finally, the scalability remains a challenge, with the necessity to produce large ceramic components with adequate properties [28].

The prospects for AM in advanced ceramic components are promising. Research is increasingly focused on using AM techniques to address key challenges in CMC fabrication, particularly in optimizing fiber-matrix interfaces and creating near-net-shape components with controlled porosity, which are crucial for aerospace and high-temperature industrial applications [28].

2.5 UV-DIW as an innovative solution

Direct Ink Writing (DIW) represents an innovative additive technology that enables the deposition of materials in ink form through a nozzle, facilitating the creation of complex structures with high dimensional precision [28]. In recent years, this technique has garnered considerable attention in the composite materials field due to its versatility and ability to produce components with complex geometries that traditional techniques struggle to achieve [29].

A significant advancement in DIW technology is UV-assisted Direct Ink Writing (UV-DIW), which combines ink deposition with UV radiation exposure, allowing rapid polymerization of the deposited material. This enhancement enables the fabrication of self-supporting structures in thin air without requiring additional supports [30].

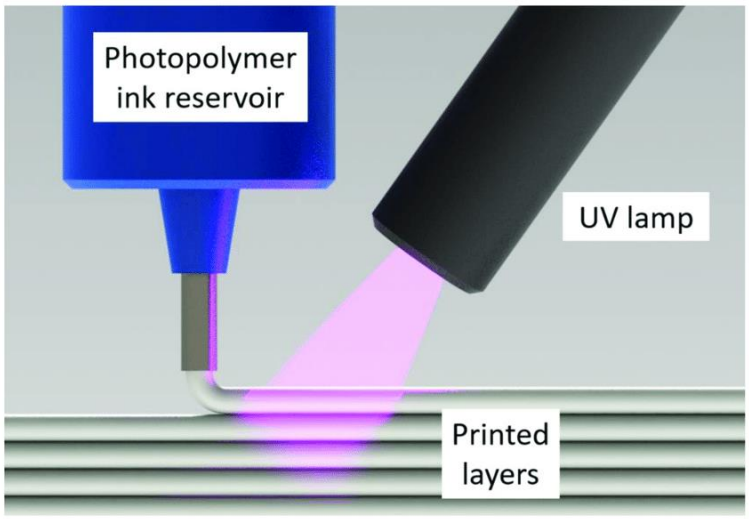

Figure 2.9. Schematic depicting the UV-DIW printing process.

The integration of a 6-axis robotic arm with UV-DIW technology constitutes a fundamental innovation that significantly increases the capabilities of this manufacturing technique. This hybrid system merges photopolymerizable ink deposition with the multi-axial movement of a robotic arm, enhancing the fabrication of three-dimensional lattice structures with complex geometries overcoming the traditional layer-by-layer limitations [31].

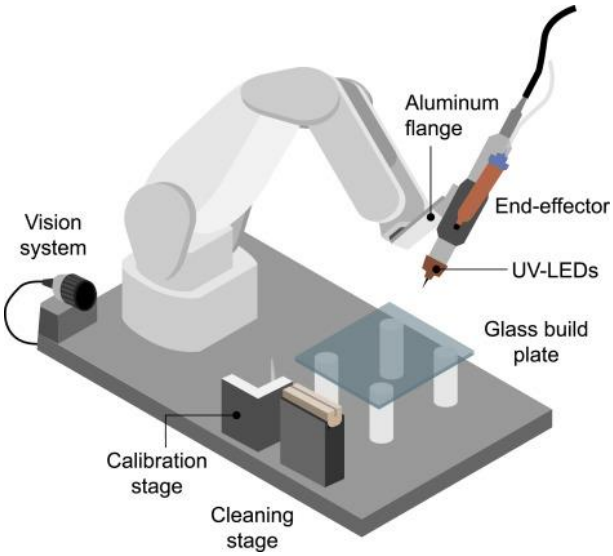

Figure 2.10. Schematic of UV-assisted DIW coupled with a 6-axis robotic arm.

A 6-axis robotic arm, unlike traditional 3D printing systems, offers precise control over nozzle orientation relative to the printing direction. This capability proves crucial for aligning fibers along the printing direction and optimizing mechanical performance by improving load distribution throughout the material [31] [32]. Furthermore, controlling nozzle orientation helps avoid interference with already printed structures a common challenge in traditional 3D printing systems that significantly limits the complexity of achievable geometries [33]. Consequently, the robotic arm's multi-axial movement capabilities, combined with the UV-curing mechanism, enable the fabrication of complex lattice structures. The robotic system's precision in ink deposition also offers higher surface finish, dimensional accuracy and manufacturing process repeatability [34].

This hybrid technology opens new possibilities for developing ceramic matrix composites with customized structures and properties. Lattice structures are particularly suitable to be designed and fabricated using this technology: thanks to the high degree of freedom of the technique, lightweight structures with tailored mechanical properties can be easily obtained [32]. The ability to precisely control fiber orientation within the ceramic matrix and create complex 3D structures with tailored properties enables the fabrication of components with higher strength-to-weight ratios and stiffness compared to conventional materials, opening new opportunities in aerospace, automotive and bioengineering fields.

Lattice and truss-based structure are emerging as highly efficient solutions for improving the strength-to-weight ratio in advanced materials. By enabling topologically optimized design, these structures

significantly improve mechanical performance while simultaneously reducing structural mass. Such configurations are widely used in high performance applications where weight reduction is crucial for energy efficiency and overall systems sustainability [35].

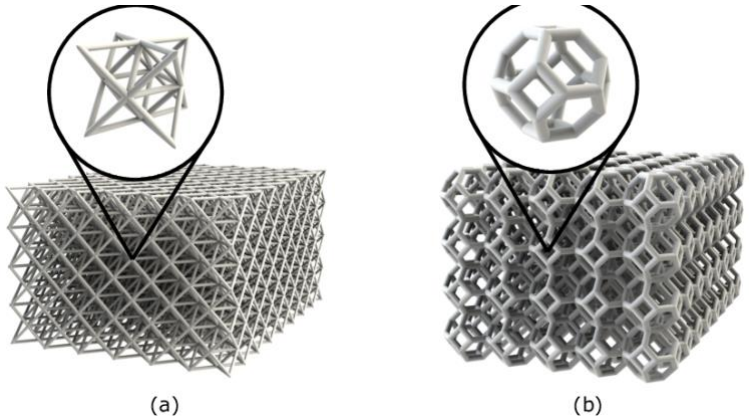

Figure 2.11. Rod-based lattice structure with (a) octet-truss and (b) Kelvin unit cell topologies.

Truss-based can be categorized in two principal types based on their mechanical behavior. The first category, known as bending dominated structures, experiences deformation primarily through flexion of structural elements, leading in comparatively lower specific resistance than their counterparts [35]. The second category comprises stretching-dominated structures, where the deformation occurs predominantly through axial loading of the trusses, guaranteeing higher rigidity and mechanical efficiency. Among these structures, the octet-truss has emerged as one of the most studied designs for advanced structural applications [36].

Integrating lattice structures into CMCs offers several advantages, including enhanced strength-to-weight ratio and optimized load distribution that minimizes stress concentration, therewith increasing mechanical resistance compared to monolithic materials [37]. The customization of mechanical properties through adjustment in relative density and the truss geometry allows precise tailoring of structural response to meet specific application requirements. Furthermore, topologically optimized configurations provide excellent capacity to absorb shock load, making them ideal for protective and energy dissipating applications [36]. [38]

Despite the advantages of AM, producing ceramic lattice structure in ceramics materials shows several challenges. One significant issue is the brittleness of ceramics, which makes connection nodes between trusses very sensible to brittle fracture [36]. Another challenge involves controlling fiber

orientation. In composite materials, the reinforcing fibers influence directly the mechanical performance. From these perspectives, the fabrication of truss-based structures using UV-assisted robot DIW represent the ideal combination.

Chapter 3
Materials and Methods

In this Chapter the experimental procedure will be presented, including the ink composition and preparation, as well as the issues related to the fabrication of the truss-based structures. Characterization of the ink and mechanical properties will be also explained.

3.1 Ink preparation

An optimal ink for the UV-DIW process should exhibit shear thinning behavior, even when loaded with a high concentration of preceramic polymers and carbon fibers, to ensure stable flow through the nozzle at moderate shear rates during printing. Additionally, it should react quickly upon exposure to UV light to maintain the shape of the extruded material.

Therefore, the ink design approach involved the selection of different reagents. First, trimethylolpropane triacrylate (TMPTA, Sigma-Aldrich, Germany) was chosen as the unique photocurable component. Its high functionality makes it highly reactive and helps in competing against the light absorption phenomena caused by the black-colored carbon fibers, consequently favoring the formation of a strong polymer network upon curing [31]. Due to its broad absorption peak in the UV light region (i.e., 400 nm) [31], bis (2, 4, 6-trimethyl benzoyl)-phenyl phosphine oxide (Omnirad 819, IGM Resins, Netherlands) was used as the photoinitiator.

Two silicone resins, Silres® MK (MK, Wacker Chemie AG, Germany) and Silres® H44 (H44, Wacker Chemie AG, Germany) were selected as preceramic polymers. During the subsequent pyrolysis in inert atmosphere, the organic structure of such polymers is decomposed, thus transforming into the ceramic matrix of silicon oxycarbide (SiOC). To ensure the complete curing of the silicone matrix prior to the complete decomposition of the organic phase, benzoyl peroxide (Luperox® A75, Sigma-Aldrich, Germany) was added to act as a thermal catalyst.

2-Propanol (Sigma Aldrich, Germany) and 2-hydroxyethyl methacrylate (HEMA, Sigma Aldrich, Germany) were chosen as solvents: due to the presence of hydroxyl groups, they are prone to form a solvation layer around the silicone powders, thus facilitating the homogeneous mixing of the components and helping into the control the viscosity of the mixture [31]. Finally, chopped carbon fibers having a length of 60 μm and a diameter of 10 μm were selected as the matrix reinforcement, while fumed silica particles (CAB-O-SIL®, Cabot, USA) were added to avoid the sedimentation of the carbon fibers in the mixture. A total of six different inks were prepared (Table 3.1). Particularly, the experimental work focused on determining the adequate ratio between the TMPTA and the silicone resins, to maximize the ink reactivity and ceramic yield. Contextually, inks were optimized to obtain a shear-thinning behavior, thus promoting continuous flow out of the nozzle.

Table 3.1. List of the different inks prepared.

Reagent (vol%)	**Ink 1**	**Ink 2**	**Ink 3**	**Ink 4**	**Ink 5**	**Ink 6**
TMPTA	18.1	18.1	18.2	22.1	21.9	21.8
Omnirad 819	0.5	0.4	0.3	1.2	1.2	1.3
Benzoyl peroxide	-	-	-	-	-	0.3
MK	76	76.1	-	-	-	-
H44	-	-	77.5	72.5	72.6	72.3
Isopropanol	5.4	5.5	-	-	-	-
HEMA	-	-	3.1	3.4	4.7	3.7
CAB-O-SIL	-	-	1.0	0.8	0.7	0.7
C fibers	9.9	25.7	5.3	9.0	8.9	8.9

The ink preparation process involved the mixing of liquid and solid components; to obtain a homogeneous paste, a centrifugal mixer (SMART DAC 250.4 VAC-P LR, Hauschild SpeedMixer, Germany) was employed. The liquid components - TMPTA, HEMA, and benzoyl peroxide - were firstly combined in a mixing cup. After that, the preceramic polymer was added in a stepwise process and incorporated into the liquid mixture. Specifically, at each step 10% of the total amount of pre-ceramic polymer was added to ensure proper dispersion and to avoid the formation of agglomerates. After each addition, the mixture was subjected to a high-speed mixing cycle for a total of 4 min, consisting of 1 min at 1500 rpm, 1 min at 1800 rpm and 2 min at 2000 rpm. All the mixing cycles were conducted under vacuum conditions (10 bar) to eliminate air bubbles and achieve a homogenous mixture.

Once all the amount of preceramic polymer was incorporated, CAB-O-SIL was added in one step to the mixture. After that, carbon fibers were gradually incorporated into the ink - each addition being 12% of the total amount of carbon fibers. Unlike the previous steps, the mixing of carbon fibers was performed without vacuum to avoid air entrapment. Lastly, Omnirad 819 was mixed into the ink with vacuum.

Finally, the obtained ink was transferred to a syringe (30 cc, Vieweg GmbH, Germany) with the help of a spatula. To avoid the presence of air bubbles during the printing process, thus avoiding the discontinuous extrusion of the ink, the syringe was centrifuge using a planetary mixer (ARE-250, Thinky, Japan) for 2 min at 2200 rpm.

3.2 Printing process

The UV-assisted Direct Ink Writing technique (UV-DIW) is an advanced manufacturing process that uses a photopolymerizable ink which is extruded through a nozzle and immediately cured by ultraviolet light. This technology allows the material to solidify in mid-air, enabling the creation of complex, unsupported 3D structure. When combined with a 6-axis robotic arm, UV-DIW further increase the degree of freedom of the system: by unlocking the additional axes, it is possible to move out from the standard 3-axis setup, thus increasing the complexity of the printable structures without being limited to a horizontal layer-by-layer approach. This setup enhances accuracy and control over the material deposition, making it easier to create intricate structures like lattices or strut-based geometries, which are characterized by a precise pin-joined frame configuration.

The printing setup is reported in Figure 3.1. It is composed of a dispensing unit extruder (vipro-HEAD 3, ViscoTEC Pumps and Dosing Technology GmbH, Germany) and UV-blocking nozzle tip (interior diameter 0.84 mm, Vieweg GmbH, Germany) installed on a 6-axis industrial robot (RV-4FRL-D, Mistubishi Electric Corporation, Japan). The aluminum support permits the connection of the extruder to the robotic flange and to maximize the robot workspace. Such support is designed to make the robot movements and avoid the collision of the printing head with the printed structure due to the encumbrance of the extruder. A syringe barrel (30cc, Vieweg GmbH, Germany) containing the ink, is connected to the dispensing unit and put under 1 bar of pressure to feed the extruder. A UV-LEDs add-on consisting of an array of 15 UV-LED chips (UV5Tz-100-15, Bivar Inc., USA), with an intensity of 50 mW cm^{-2} measured at a wavelength of 400, at the point of extrusion is attached at the extremity of the extruder. Such UV-LEDs are uniformly distributed on the spaced around the nozzle tip of the extruder using a custom 3D printed add-on.

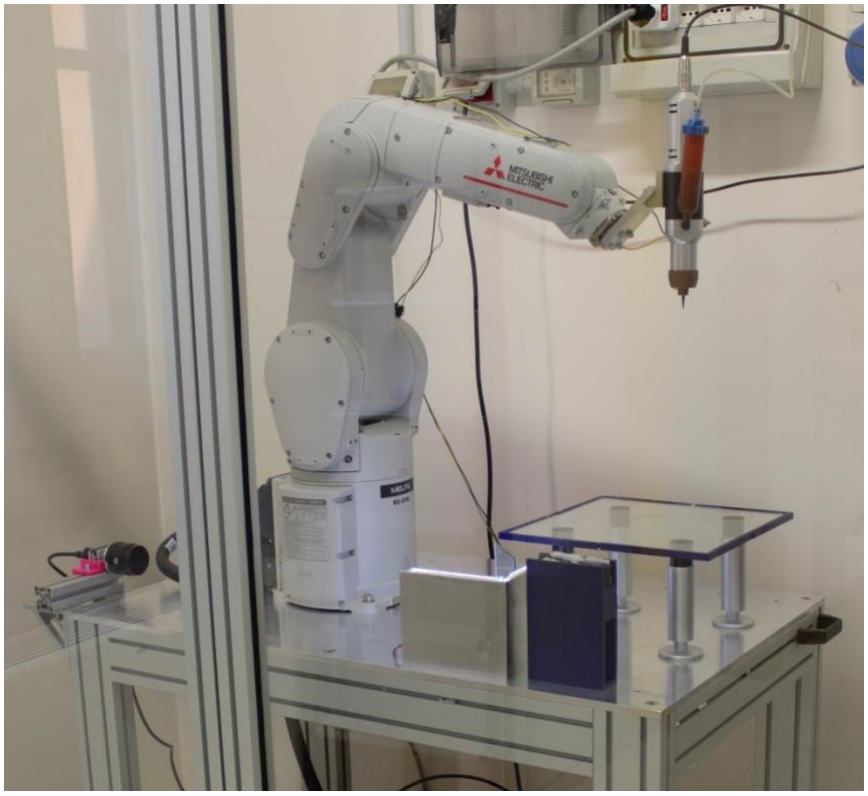

Figure 3.1. Robot hybrid UV-DIW setup.

In this project, truss-based structures were designed using a repetitive unit cell configuration known as FCCZ (Face-Centered Cubic with Z-axis support). This cell type was selected for its ability to distribute loads effectively across the structure, enhancing the overall strength while minimizing weight [31]. The FCCZ unit cells are characterized by diagonals on each face of the cells itself, which contributes to the rigidity and beading resistance capacity of the structure. The beams fabricated using this technology are composed of five FCCZ unit cells, providing final dimensions of 70x14x14 mm^3 (l x w x h) (Figure 3.2)

Due to the non-continuous printing process of the robot assisted UV-DIW technology used, the printing path was designed using the Rhino3D modelling software (2020, Rhinoceros 6, Robert McNeel & Associates, USA) and its graphical scripting editor, Grasshopper (2024, Grasshopper3D, Robert McNeel & Associates, USA). For the different truss-based components shown in this work, the printing speed range was defined between 0.5 mm s^{-1}.and 1.5 mm s^{-1}.

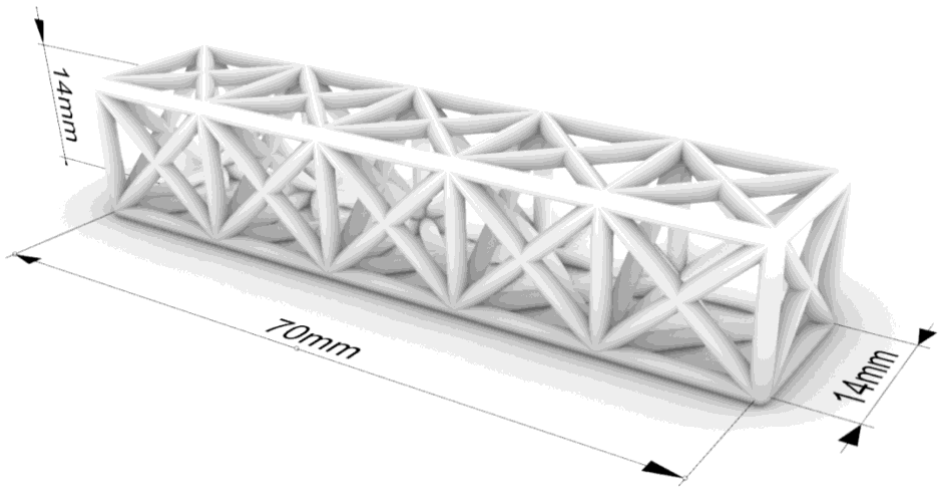

Figure 3.2. Rendered image of the FCCZ truss-based model.

3.3 Characterization of ink and sintered samples

The rheological behavior of the ink was analyzed using a rotational rheometer (Kinexus Lab+; Netzsch, Germany.). The instrument was equipped with a 20 mm head geometry and gap of 0.2 mmm was selected; measurements of shear stress and viscosity were performed over a shear rate range of

0.1 s^{-1} to 250 s^{-1}. For photo-rheological characterization, a UV-plate system accessory (KNX5007, Netzsc, Germany) with a 94-mW cm^{-2} UV lamp was used.

A micrometer screw gauge was used to determine the curing depth of the suspension and the thickness of the cured section of ink droplets irradiated by the UV-LED at varying exposure times (with the light intensity constant at 94 mW cm^{-2}). The corresponding energy densities were calculated as the product of light intensity and exposure time.

The Archimedes test method was employed to analyze the open porosities, apparent and bulk density (Sartorius 1801, Sartorius GmbH Göttingen, Germany). To fit the instrument, FCCZ unit cells were designed, fabricated and used instead of the beam structure. The test process was carried out for 6 different samples.

Scanning Electron Microscope (SEM) (CUBE II, EmCrafts Co., Ltd., Republic of Korea) was used to assess the alignment and distribution of the carbon fibers within the filaments of the final structures.

In this study, a universal testing machine (Quasar25, Galdabini Cesare S.p.A., Italy) was employed to perform the test according to specific parameters. The crosshead speed was set at 0.7 mm min^{-1} and a pre-load of 0.3 N was applied to ensure proper contact before starting the test. The test-end mode was configured to stop when the force dropped below 95% of the maximum force, indicating failure. A support distance of 45 mm was used, and the four-point bending configuration was set to L/3. The testing machine recorded force and displacement data, providing the mechanical behavior of the truss under bending.

3.4 Sample characterization

Optical microscope (AxioCam ERc 5s Microscope Camera, Carl Zeiss Microscopy, Thornwood, USA) and ImageJ software were used with the specific aim of guiding the optimization of the AM. Microscopic analysis allowed the precise determination of the relationship between the print parameters and the dimensional characteristics of the truss-based structure, which is a critical aspect considering the significant volumetric shrinkage during the sintering. Using this analysis, it was possible to quantify the dimensional reduction of the filaments during the various process steps. This

information was fundamental for modifying the initial design of the truss-based to account for shrinkage and the sintering treatment was optimized to obtain the desired final dimensions.

Analysis using ImageJ allowed quantification of the efficiency of the different infiltration steps, monitoring the progressive reduction of open pores and correlating these data with the mechanical properties of the final structures [39]. This approach was decisive to determining that the infiltrations steps represented the optimal solution to densify the truss-based structures.

3.5 Heating treatments and liquid infiltration process

To eliminate the organic phase and promote the full densification of the printed structures, all samples were thermally treated. Specifically, the thermogravimetry analysis (TGA, SDT650 0650-0843, TA Instruments, USA) was carried out in nitrogen atmosphere from room temperature to 1000 °C, with a heating rate of 10 °C min^{-1} and it was utilized to design the heating schedule. Figure 3.3 shows the TGA curve of Ink 6 referred to Table 3.1. As displayed, the curve initially shows a slight weight loss (~5%) up to 250°C: this loss can be attributed to the volatilization of residual solvents, moisture, and any unreacted monomers, such as HEMA and TMPTA, within the ink matrix. The minimal mass loss in this region indicates that the ink components remain largely stable until the onset of more significant thermal events.

A huge weight loss (~20%) occurs between 258°C and 466°C, marking the major decomposition phase of the ink. This region corresponds to the degradation of organic components, including TMPTA and HEMA, which are expected to decompose at these temperatures. Additionally, the decomposition of benzoyl peroxide may contribute to the mass loss observed in this range. The sharp peak of the first derivative curve around 466°C indicates a rapid weight loss, likely due to begins to form SiOC. Following the first huge decomposition phase, a secondary weight loss is observed around 590°C. This is characterized by a smaller weight loss, which may be attributed to the continued degradation of residual organic component. Once it exceeds 600°C, there is a gradual reduction in weight. This final weight loss indicates the complete transition to a fully ceramic SiOC structure. By this stage, all the organic content has been decomposed, and the remaining material primarily consists of an inorganic SiOC matrix, reinforced by the presence of carbon fibers and silica.

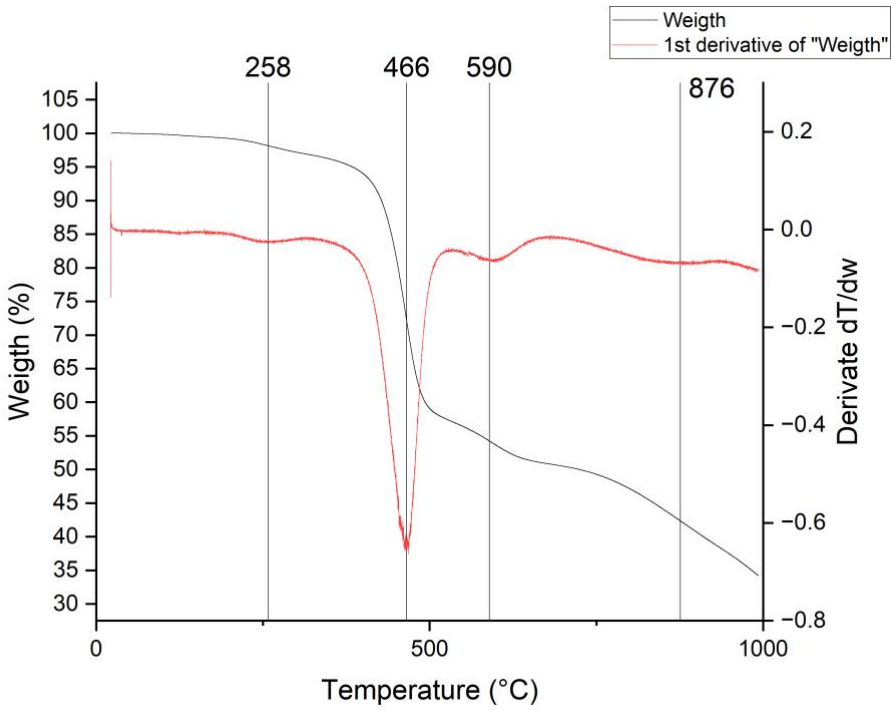

Figure 3.3. TGA curves of the different reagents composing the ink.

Therefore, the heating schedule was designed as follows: 5 °C min^{-1} from 50°C to 200°C, 1 °C min^{-1} from 200°C to 300°C, with a holding time of 1 hour, 1 °C min^{-1} from 300°C to 420°C and a holding time of 2 hours, 1 °C min^{-1} from 420°C to 600°C and a holding time of 1 hour, and finally 2 °C min^{-1} from 600°C to 1000°C and a holding time of 1 hour. All the printed structures were thermally treated in a tube furnace with a controlled flow of N_2 of 0.1 L min^{-1}.

Due to the differential shrinkage of the matrix and reinforcement, preliminary thermal treatments highlighted the presence of transversal cracks in the trusses. To tackle this issue and enhance densification of the SiOC trusses, a multi-step infiltration process was employed. The infiltration solution was prepared by mixing H44 with 2-propanol in proportion 1:1, thus obtaining a quite low viscous mixture. Indeed, preliminary tests showed that higher H44 concentration lead to an increase of the viscosity of the infiltration solution, consequently making it difficult to flow inside of the open porosities present on the surface of the sintered structures.

The infiltration of the SiOC truss was carried out through a controlled multi-step process to maximize the penetration of the resin into the porous structure and ensure the closure of open pores. The phases of the infiltration process were the following: (i) sintered structures were immerged in the infiltration

solution and subsequently vacuumed for 10 minutes; (ii) structures were removed from the infiltration solution and placed in the oven at 60°C for 1 h to ensure the isopropanol evaporation and curing of the preceramic polymer, and (iii) heat treatment. To ensure the complete filling of the pores, such three steps were repeated two times, for a total of 2 infiltrations and 3 sintering processes.

Chapter 4
Results and discussion

This Chapter presents the experimental results obtained in this study, including the rheological characterization of the ink, microstructural images, optimization of sintering treatments, and the mechanical characterization of the carbon fiber reinforced SIOC matrix composite truss-based structures.

4.1 Ink design and lattices fabrication

According to the power law model, the rheological behavior of a non-Newtonian fluid can be described by (1):

$$\sigma = K\, g^n \quad (1)$$

Where K represents the material consistency, n is the flow exponent, while σ and γ are respectively the shear stress and shear rate. Specifically, K is an indicator of how much stress is needed to be applied to the fluid to make it flow; by that, higher values of K (i.e., over 800 Pa s^n [40]) are expected for very thick pastes loaded with ceramic particles. On the other hand, n determines the rheological nature of the ink: n=1 corresponds to a Newtonian fluid, n>1 indicates a shear-thickening behavior, while n<1 represents a shear-thinning fluid.

The rheological analysis reported in Figure 4.1 shows the variation of shear stress and viscosity as a function of shear rates. By interpolation with (1) it is possible to obtain characteristic values of K=61.9 ± 1.2 Pa s^n and n=0.8 ± 0.004 (R^2=0.99), therefore confirming the non-Newtonian and shear thinning behavior of the formulated ink, well aligned within the process requirements. It should be highlighted that the value of n is close to 1, thus suggesting a fluid behavior that approaches Newtonian characteristics. This observation is supported by the moderate variation of viscosity – approximately 3 Pa s – across the wide range of the shear rate tested (i.e., from 0.1 to 300 s^{-1}).

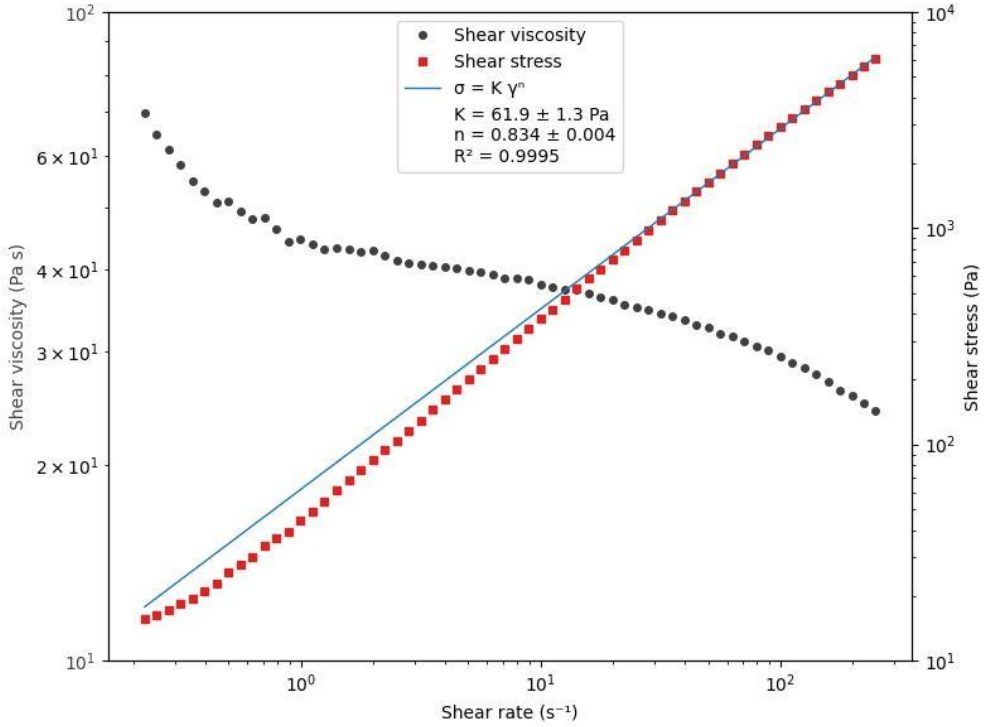

Figure 4.1. Rheological behavior of the ink 6 as function of shear rate.

To investigate the influence of the UV light on the rheological properties, loss modulus (G") and the storage modulus (G') were analyzed as a function of time, while the UV light was switched on after 50 s and kept on for over 150 s until the modulus reached a plateau. As displayed in Figure 4.2, initially the material exhibits typical liquid-like behavior since G" is constantly higher than G', indicating the predominance of the viscous component over the elastic behavior and thus a poor ability of the ink to maintain printed shape. While not desired for traditional DIW, such characteristic is not detrimental for the UV-DIW process: the tailoring of the curing process by the UV light can help in retain the filament structure. Indeed, G' increases as the UV light is switched on, passing from 10^3 Pa to 10^7 Pa, overcoming G", highlighting the transformation to solid-like behavior. This behavior is consistent to that reported by Huang et al., where the shear modulus increases rapidly upon UV activation until reaching 10^7-10^8 Pa [41]. In both cases, this increase in the elastic modulus is fundamental to guaranteeing the self-support of the printed structure. While the crossing point of G" and G' happens after 40 s from the switching on of the UV radiation, both values surpass their initial ones and become very similar to each other just after 10 s (Figure 4.2). This correlates well within the printing parameters used: trusses with a variable length of 10 mm and 14 mm were printed at a speed of 1.5 mm s^{-1}, depending on the point of the structure, therefore requiring approximately 9 s to be fabricated. By that, the results obtained confirm the suitability of the formulated ink for UV-DIW

applications, highlighting its rapid curing and capability of the structures to maintain their shape after extrusion.

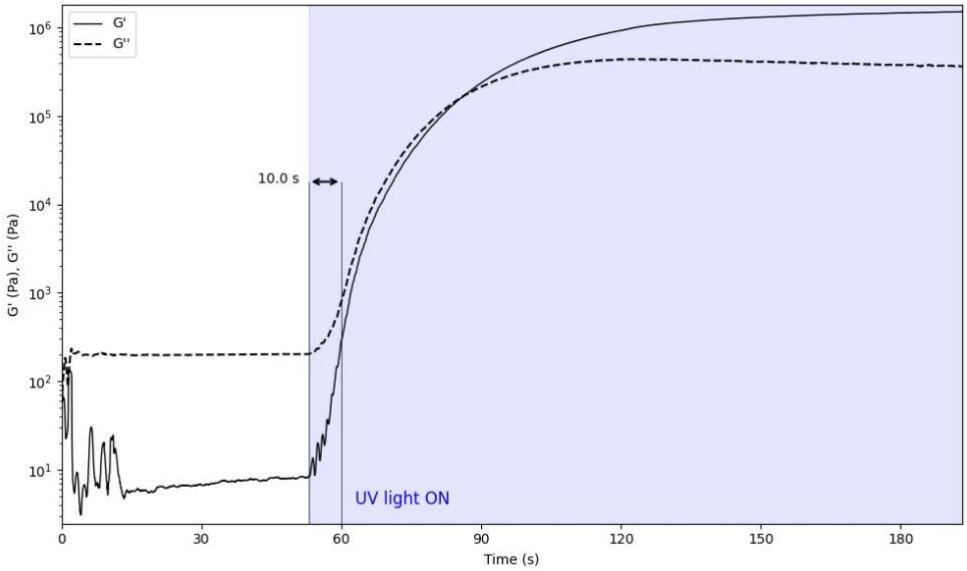

Figure 4.2. Crosslinking of the ink after and before UV irradiation.

The curing depth of the ink represents a key parameter of UV-DIW process, as it directly influences the possibility to obtain self-supported structures [41]. An in-depth knowledge of the relation between UV energy and the cure depth is essential to determine the correct calibration of the process parameters, such as the print velocity and the UV radiation intensity [31]. The interaction between these parameters determines the capability of the ink to maintain its geometry after extrusion, allowing the fabrication of complex support-less structures. As illustrated in Figure 4.3, the experimental data follow a power law relationship, expressed by the Jacobs equation:

$$C_d = D_p \ln\left(\frac{E}{E_c}\right) \tag{2}$$

where C_d represents the curing depth, E is the energy density at the filament surface, D_p is the penetration depth of the ink, and E_c is the critical energy dose [42]. The curing depth obtained as a function of UV energy shows a non-linear trend that provides valuable insights into the photopolymerization behavior of the carbon fiber-reinforced ink.

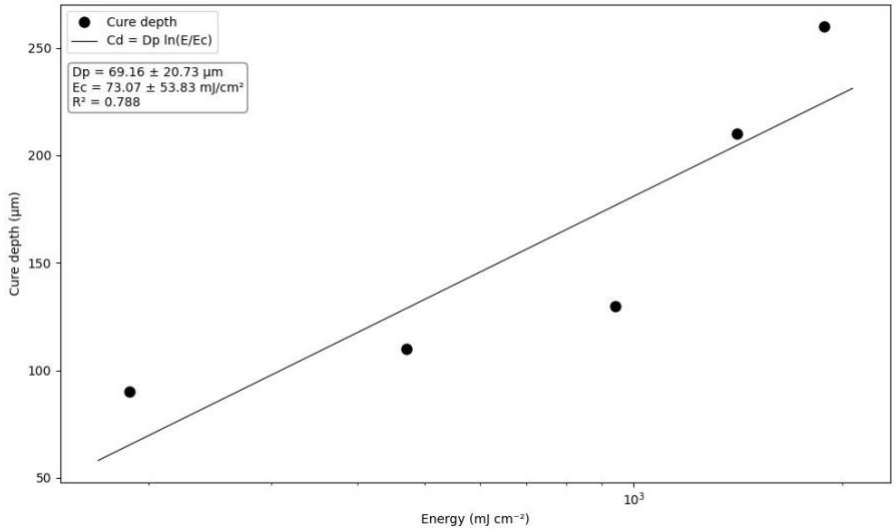

Figure 4.3. Cure depth of the ink as a function of energy.

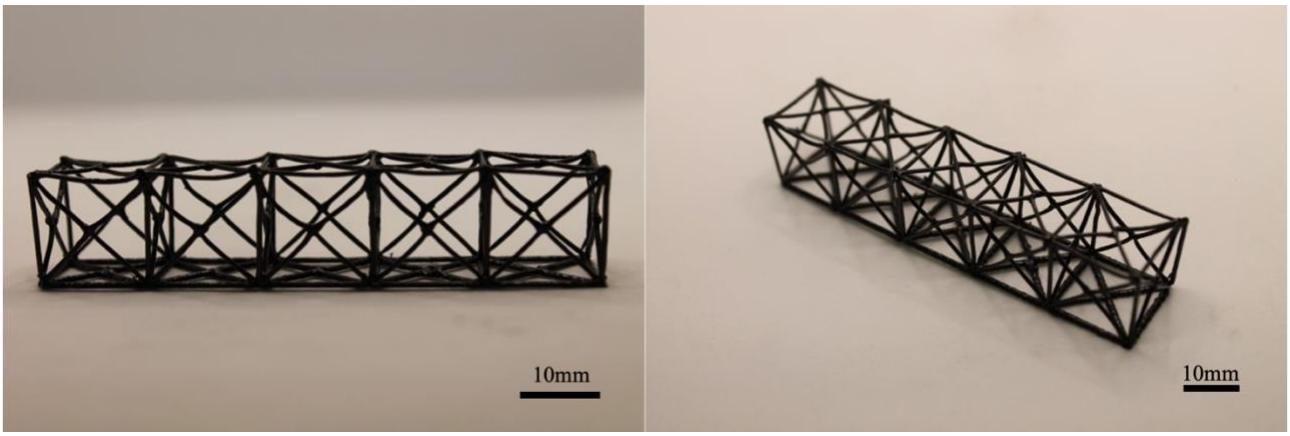

Figure 4.4. Truss-based FCCZ lattice post print

The characteristic values determined by this analysis are: D_p=69.2 ± 20.7 µm and E_c=73.1 ± 53.8 mJ cm^{-2} (R^2=0.788). Comparing these values with those reported in literature [41] for a system based on H44 and PETTA (D_p=560 µm and E_c=50.6 mJ cm^{-2}), it is possible to notice significant differences. First, the black coloration of the carbon fibers acts as a barrier to UV irradiation, limiting the penetration depth of the light in the deeper regions of the materials [23]. On the other hand, similar E_c values suggest that more energy is necessary to initiate the curing process. Nonetheless, as proved by the printed samples reported in Figure 4.4, it is not actually necessary to completely cure the ink (i.e., D_p=420 µm, half of the nozzle diameter used for printing) to enable maintaining the printed shape. In fact, the rapid polymerization of the outer shell of the extruded filament at the beginning helps to provide self-supporting ability, while the printing speed can be tailored to couple with the degree of curing [31].

4.2 Post-treatments and characterization

The comparison between the theoretical dimensions of the 3D model and the actual measurements of the truss-based structures provides important information on the dimensional accuracy and quality control of the UV-DIW technique coupled with a 6-axis robotic arm. The theoretical dimension of the printed beam structures, considering also the diameter of the trusses, were of 70.8x14.8x14.8 mm^3. As shown in Table 4.1, the post print measurements highlight excellent correspondence with the theoretical dimensions. These results confirm the accuracy of the truss-based structures fabrication using UV-DIW technology coupled with a 6-axis robot arm.

Table 4.1. Measurements of truss-based structures.

Process steps	Length (l) (mm)	Width (w) (mm)	Height (h) (mm)
Post print	71.1 ± 0.4	14.8 ± 0.2	15.0 ± 0.2
1st sintering	68.3 ± 0.7	14.1 ± 0.7	14.2 ± 0.4
2nd sintering	68.1 ± 0.6	14.1 ± 0.3	14.0 ± 0.4
3rd sintering	67.6 ± 0.6	14.1 ± 0.3	14.1 ± 0.3

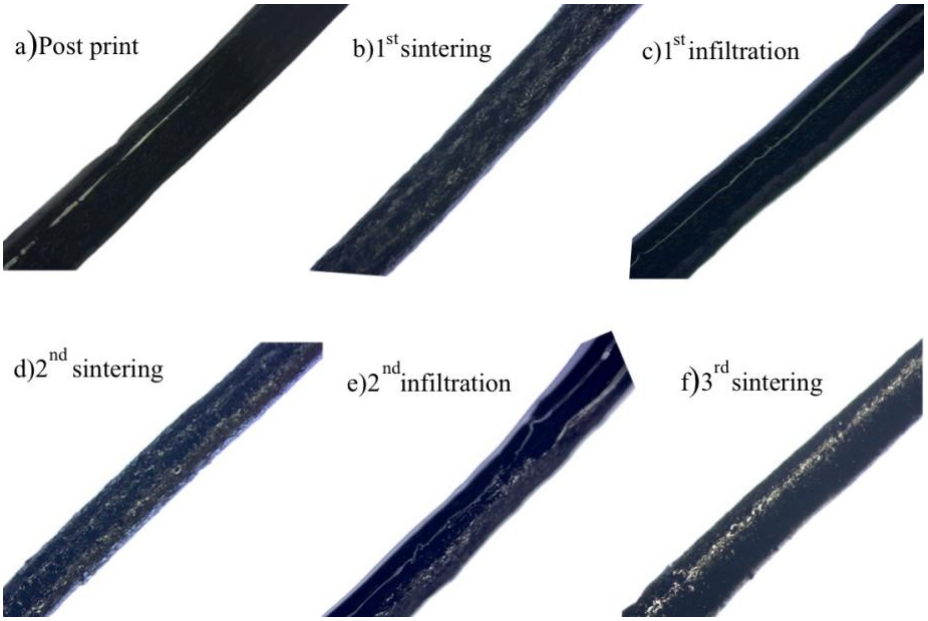

Figure 4.5. Microscope images of the 6 steps of the fabrication process: post print, 1st sintering, 1st infiltration, 2nd infiltration, 2nd sintering, and 3rd sintering (a-f).

The subsequent sintering and infiltration steps led to a progressive dimensional change, with significant shrinkage observed particularly after the first sintering. The length decreased by 4%, while the width and height decrease by 4.7% and 5.3%, respectively. The filament thickness showed significant reduction, passing from 784 ± 78 µm to 554 ± 50 µm (Figure 4.6). These dimensional variations are consistent with the volumetric shrinkage due to decomposition of the organic components and the consequent densification that occurs during the ceramic conversion process between stage 1 and 2. On the other hand, no significant dimensional variation can be noted from stage 3 onwards, suggesting that the infiltration liquid was able to penetrate the porosities without increasing the thickness of the trusses, as can be noticed in Figure 4.5 and Figure 4.6.

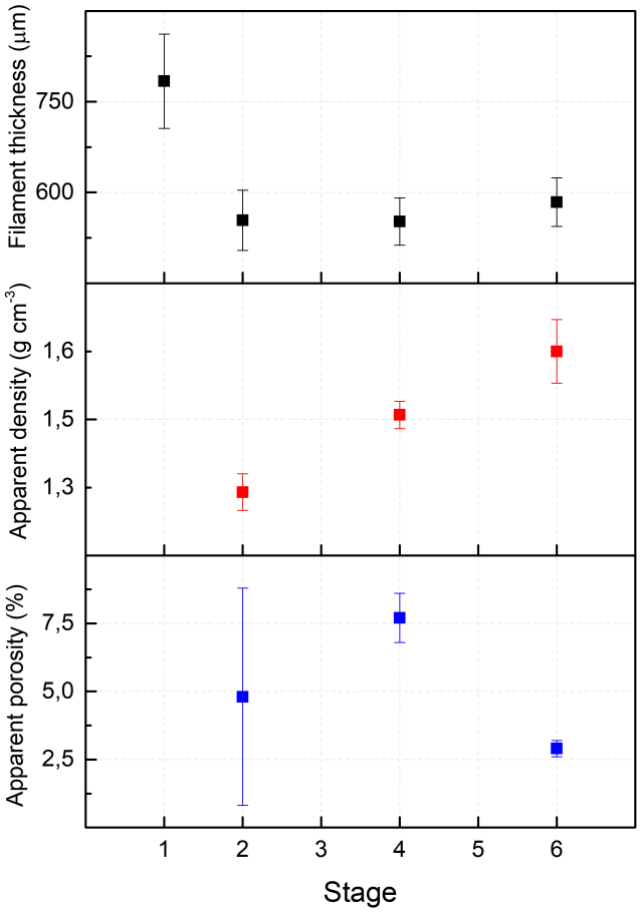

Figure 4.6. Filament thickness, apparent density and porosity evolution of the filaments during the different stages of the post treatment.

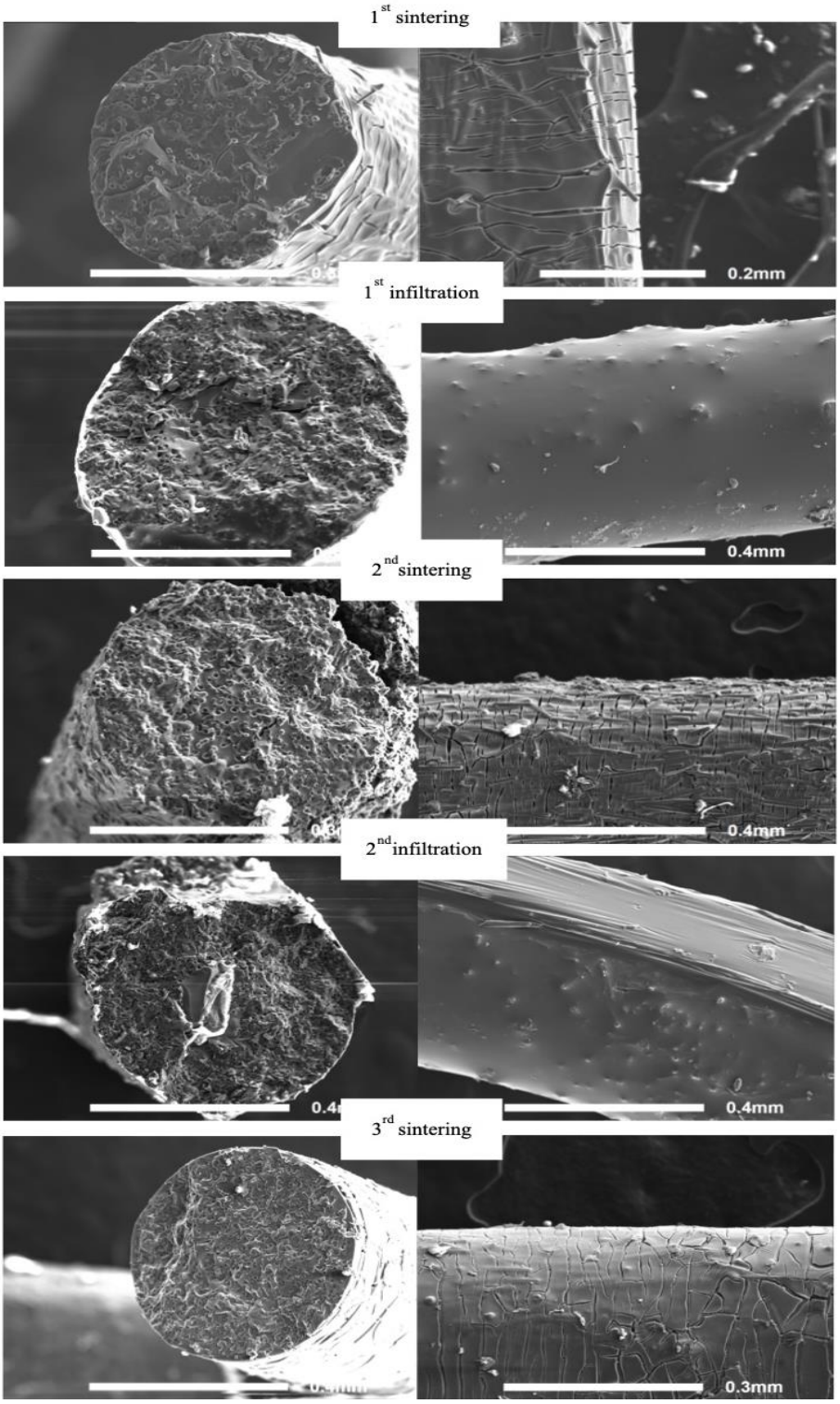

Figure 4.7. SEM image of the 5 steps after the 1st sinterng,1st infiltration, 2nd infiltration, 2nd sintering, and 3rd sintering.

Figure 4.7 reports the morphological evolution of the trusses cross-section and surface during the six stages of the post treatments. The first thing to highlight is the preferential alignment of the carbon fibers along the extrusion direction which can be noted in all the steps. This phenomenon can be attributed to the shear forces generated during the printing process, which cause the fibers to orient with the direction of material flow through the nozzle. This alignment of the fibers leads to significant anisotropy in the mechanical properties of the composite trusses, specifically enhancing the strength along their axes and thus the fracture toughness of the overall final structure. Such control over the fiber's orientation represents a significant advantage of the UV-DIW technique coupled with 6-axis robotic arm compared to conventional layer-by-layer AM approaches.

As expected, the differential shrinkage between the matrix and fibers led to the formation of transversal cracks with respect to the truss axis after stage 2 (Figure 4.7). Despite such defects, the cross-sectional area is dense and the chopped carbon fibers are homogeneously distributed. From this perspective, it should be also highlighted the absence of closed porosities within the matrix/fiber interface, thus suggesting the safe removal of the organic phase and confirming a well-tailored heating schedule as well as a strong bonding between the two phases. The SEM images of the 1st infiltration cycle confirm the successful filling of the cracks and the formation of an additional preceramic polymer layer around the filament surface which is later transformed into SiOC after the 2nd thermal treatment (Figure 4.7). Unsurprisingly, the latter step leaves behind a non-dense coating deriving from the low ceramic yield of the infiltrating solution (i.e., 41 wt%, considering that the preceramic polymer corresponds to 50 wt% of the solution and its theoretical ceramic yield is 82 wt%). Such morphological changes are reflected by the results of the Archimedes analysis: as reported in Figure 4.6, the apparent density gradually increases after each PIP cycle, therefore suggesting the efficient filling of the open porosities present on the filaments surface.

On the other hand, the evolution of the apparent porosity does not show a unique trend and should be discussed in its singular stages. The presence of open porosity in ceramic materials significantly influences their mechanical performance and functional properties. The presence of open pores can compromise the mechanical strength of the material, while their closure contributes to improving structural cohesion. Therefore, reducing open porosity through controlled infiltration is an effective strategy to improve the mechanical performance of SiOC components ([43]). After the 1st sintering (stage 2) the porosity is relatively high and with a high value dispersion: this can be attributed not only to the polymer-to-ceramic conversion but especially to the presence of errors and defects arising

from the printing process. Such high variability is later decreased in stage 4 as the infiltration step enabled the formation of a uniform coating; yet the porosity remained high (i.e., 7.5 %) due to the formation of additional cracks. This phenomenon can be due to greater accessibility of internal cavities following the first infiltration step. The initial infiltration step partially saturates the porous structure, potentially modifying the surface tension characteristics within the pores and influencing the penetration dynamics of the infiltration solution in subsequent treatments. As the PIP cycle is repeated another time (stage 6), there is a strong decrease in the apparent density (i.e., of about 1/3 with respect to the one in stage 4) which is probably related to the efficiency of the 2nd infiltration step. Such result is consistent with what is typically expected in traditional PIP procedures: the higher the number of cycles, the lower the apparent porosity ([44]).

The results obtained for the density and porosity measurements confirm that the multi-step infiltration leads to a denser and less porous material, which are the principal characteristics for improving mechanical performance of CMCs. Furthermore, the reduction of open pores is a key element to increae resistance to crack propagation, a main aspect for advanced structural applications ([45]).

4.3 Four-Points Bending Test

In fiber-reinforced CMCs, fiber toughening is crucial. The strength of the matrix-fiber interface significantly influences this toughening. A strong interface leads to direct crack propagation through the fibers, resulting in premature failure and low toughness. Conversely, a weak interface promotes debonding, crack deflection, bridging, and fiber pull-out, enhancing toughness and enabling gradual failure. Regardless of the material, the mechanical behavior of a certain component can be tailored by optimizing its geometry, specifically designing stretch-dominated architectures like the one proposed in this work. Indeed, as reported by Huang et al. [41], the flexural behavior of SiOC-based sandwiches is characterized by a linear elastic deformation followed by minor failures which strongly depends on the progressive failure of the joining points between the trusses.

To assess the mechanical properties, the carbon fibers/SiOC truss-based structures have been evaluated trough the four-points bending test. Figure 4.8 displays the load-displacement curves obtained from eight samples, with the red curve which represents the average response. The curve shows the expected failure behavior: as the crosshead moves downwards, the structure begin to

deflect until breaking at one of the joints, thus reaching a major drop in the load profile. After that, failures propagated, leading to the rupture of more joining points.

The cross section of the 3rd sintering reported in Figure 4.7 is characteristic of one trusses of a truss-beam structure after the bending test. As can be seen, there is no significant fibers pullout, thus suggesting the formation of a strong matrix/fiber interface which did not hinder the failure mechanisms described. To better define the effect of the fibers on the mechanical properties, tensile tests on single mini-composites filaments should be carried out. Nonetheless, such work was not conducted as it was out of the scope of the present research activity.

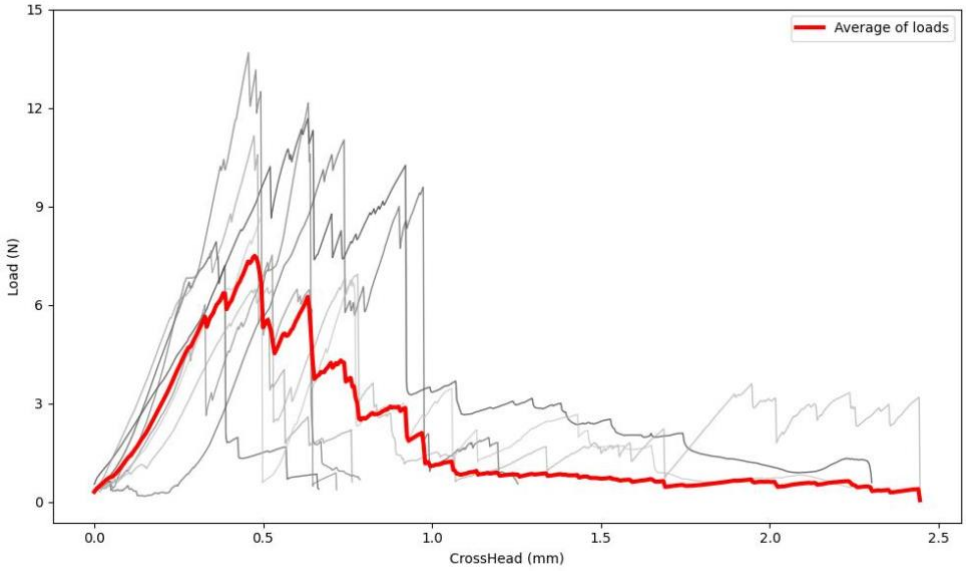

Figure 4.8. Load-Displacement curves for four-points bending tests of truss-based structures.

The maximum load values, ranging from 7 N to 14 N, show a significant dispersion. This variation can be attributed to the microstructural heterogeneity intrinsically introduced during the fabrication process, due to factor such as the presence of residual porosity and defects formed during the thermal treatment. Based on the weakest link postulate, the Weibull distribution function is commonly utilized for the statistical analysis of ceramic mechanical properties, determining the likelihood of failure at a specific load. Such statistical distribution can be described by:

$$F = \frac{m}{F_0}\left(\frac{F_{max}}{F_0}\right)^{m-1} e^{-\left(\frac{F_{max}}{F_0}\right)^m} \quad (3)$$

Through the linear-regression method it is possible to plot the fracture load values as a function of their probability of failure, thus obtaining the graph shown in Figure 4.9, which reports the statistical distribution of the measured failure load of 8 different samples. By fitting of a linear curve, it is possible to estimate m (i.e., slope of the curve) and F_0 – instead, representing the characteristic failure load – which is the y-intercept at P = 63.2 %, thus obtaining characteristic values of m =4.29 and F = 10.8 N (R^2 = 0.961).

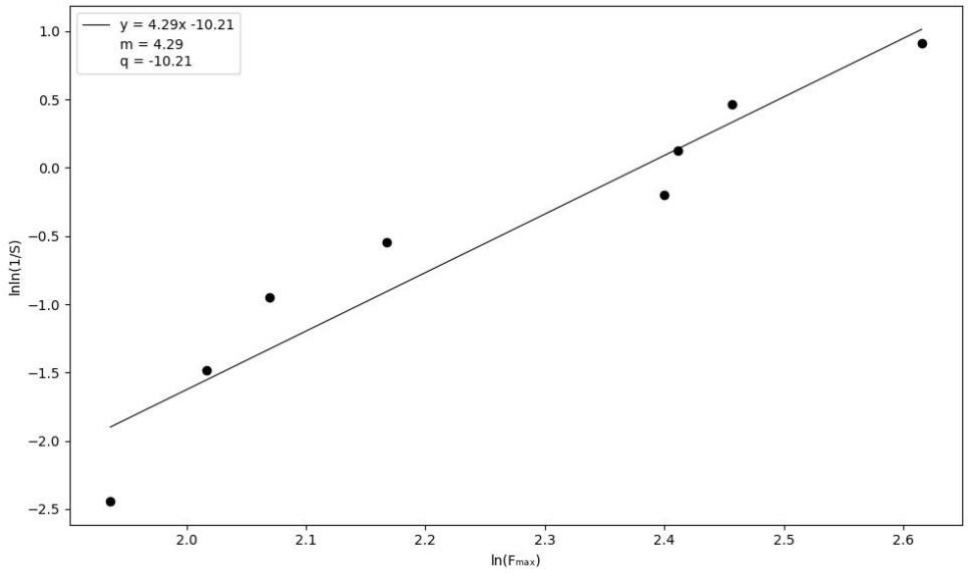

Figure 4.9. Linear Weibull Distribution

The Weibull modulus is particularly informative when compared with the values in literature for similar ceramic materials. Huang et al. ([46]), for example, have reported a Weibull modulus of 2.36 for SiOC scaffolds fabricated with DIW with total porosity of about 88%. Osuchukwu et al. ([47]), instead, have obtained values from 3 to 8 for SiOC structures fabricated using an AM technique, with the lower values corresponding to the complex geometries and high level of porosity. The values of m reported falls within this interval and is reasonable considering the complexity of the FCCZ truss-based and the challenges associated with production using UV-DIW coupled with 6-axis robotic arm. The relatively low Weibull modulus indicates considerable variability in the strength distribution, which can be attributed to the presence of defects induced during the fabrication process and residual open pores in the structures. This level of variability is acceptable considering that the design of the end effector is prone to manufacturing errors in all 6 degrees of freedom of the tool transformation

matrix (both displacements and rotations) since none of the tool reference frame axes is aligned with the robot axes [31].

The mechanical performance observed in the samples, while showing moderate variability, demonstrates that the UV-DIW coupled with 6-axis robotic arm technique can produce carbon fibers/SiOC structures with predictable failure statistic. The intrinsic open pores influence the mechanical properties variability, as evidence from Weibull modulus, but the load-bearing capability remains within an acceptable interval for potential structural applications ([48]).

Chapter 5
Conclusions

This thesis successfully demonstrated the feasibility of fabricating carbon fiber-reinforced SiOC truss-based structures using UV-assisted Direct Ink Writing (UV-DIW) coupled with a 6-axis robot arm. This innovative approach effectively addresses limitations associated with traditional additive manufacturing techniques for ceramic matrix composites.

The rheological properties of the ink were optimized to ensure suitability for the UV-DIW process. The ink exhibited non-Newtonian, shear-thinning behavior, facilitating consistent material flow during extrusion. The rheological analysis confirmed also the efficient photo-crosslinking under UV exposure, with a clear transition from a viscous to a solid-like response. While carbon fibers influenced UV penetration and curing depth, the ink demonstrated adequate curing for shape retention during printing.

Microstructural analysis revealed significant anisotropic shrinkage in the filaments following the initial sintering step. Subsequent steps led to dimensional stabilization. SEM analysis confirmed the desired fiber alignment along the extrusion direction, a key feature of this technique that contributes to enhanced strength and stiffness along the filament axis. TGA analysis facilitated the development of a controlled sintering process, where slower heating rates in critical temperature ranges effectively managed organic component decomposition and SiOC phase formation.

A multi-step infiltration process proved effective in reducing open porosity from 4.8% after the first sintering to 0.9% after the final infiltration and sintering steps. Simultaneously, the apparent density increased from 1.34 g cm^{-3} to 1.65 g cm^{-3}, indicating a progressive reduction in open porosity and the achievement of denser structures. These results highlight the importance of controlled multi-step processing for achieving high-performance CMCs.

Mechanical characterization, using four-point bending tests and Weibull analysis, provided insights into the structural reliability of the composites. The Weibull modulus indicated a moderate level of

data dispersion, considered acceptable given the geometric complexity of the truss structures and the inherent challenges of their fabrication. The failure rate exhibited an exponential increase underload, suggesting a failure mechanism driven by critical defects and rapid crack propagation.

In summary, this study successfully fabricated SiOC truss-based structures reinforced with carbon fibers using UV-DIW and a 6-axis robotic arm. The optimized ink formulation, controlled printing process, and effective post-processing steps led to the production of complex CMC structures with controlled microstructure and improved density. While the structures demonstrated moderate strength, the study provides a foundation for further optimization and application of this advanced manufacturing technique for CMCs.

5.1 Future Work

The results obtained in this thesis work suggest several directions for future research. First, the ceramic yield of 70% obtained in our case study with the Silres® H44 represents a value that could be further optimized. Future research could focus on improving this parameter by modifying the preceramic polymer or, alternatively, on incorporating specific particles into the initial formulation. These particles could help reduce the characteristic porosity of components fabricated via AM, consequently improving the final mechanical properties. A second area of development concerns the full exploitation of the capabilities offered by the 6-axis system used in this study. Thanks to enhanced design freedom, it could be possible to create functionally graded structures, consisting in regions with low porosity and high density (i.e., trusses touching, parallel to each other) and regions with higher porosity and lower density (i.e., lattice-like geometries). This approach would allow the fabrication of structures with optimized stress distribution and specifically improve the ratio between mechanical performance and component weight. Finally, the implementation of finite element analysis (FEM) would represent a fundamental step in understanding the flexural mechanisms observed in the studied samples. These simulations would allow correlation of the material's microstructure with macroscopic behavior, providing valuable guidance for optimizing design and process parameters.

References

[1] W. Krenkel, Ceramic Matrix Composites, KGaA, Weinheim: WILEY-VCH Verlag GmbH & Co., 2008.

[2] J. Wong, A. Altassan and D. W. Rosen, "Additive manufacturing of fiber-reinforced polymer composites: A technical review and status of design methodologies," vol. Composites Part B 255, no. 17, 2023.

[3] E. Bernardo, L. Fiocco, G. Parcianello, E. Storti and P. Colombo, "Advanced Ceramics from Preceramic Polymers Modified at the Nano-Scale: A Review.," *Materials,* vol. 7, no. 1927–1956, 2014.

[4] F. Sarraf, S. Churakov and F. Clemens, "Preceramic Polymers for Additive Manufacturing of Silicate Ceramics.," *Polymers,* vol. 15, no. 4360, 2023.

[5] P. Colombo, G. Mera, R. Riedel and G. Sorarù, "Polymer-Derived Ceramics: 40 Years of Research and Innovation in Advanced Ceramics.," *Journal Am. Ceramarics Society,* vol. 93, no. 1805–1837, 2010.

[6] E. Bernardo, P. Colombo and S. Hampshire, "Advanced ceramics from a preceramic polymer and nano-fillers.," *Joulnel Eurpean Ceramics Society,* vol. 29, no. 843–849, 2009.

[7] P. Colombo, E. Bernardo and G. Parcianello, "Multifunctional advanced ceramics from preceramic polymers and nano-sized active fillers," *J. Eur. Ceram. Soc.,* vol. 33, no. 453–469, 2013.

[8] P. Greil, "Polymer derived engineering ceramics.," *Advance Engineering Matererials,* vol. 2, no. 339–348, 2000.

[9] S. Fu, M. Zhu and Y. Zhu, "Organosilicon polymer-derived ceramics: An overview.," *J. Adv. Ceram.,* vol. 8, no. 457–478, 2019.

[10] M. Singh and R. Asthana, "Advanced Joining and Integration Technologies for Ceramic Matrix Composite Systems.," in *W. (ed.) Ceramic Matrix Composites.*, Weinheim, Wiley-VCH Verlag GmbH & Co. KGaA, 2008, pp. pp. 303-324.

[11] W. N. R. a. S. H. Krenkel, "High Temperature Ceramic Matrix Composites," in *Ceramic Matrix Composites*, Weinheim, Wiley-VCH Verlag GmbH & Co. KGaA, 2001.

[12] E. S. Nelson and P. Colella, "Parametric Study of Reactive Melt Infiltration," 2000.

[13] R. Naslain, "Ceramic Matrix Composites: Matrices and Processing," *Encyclopedia of Materials: Science and Technology,* vol. 1, pp. 1060-1066, 2001.

[14] F. Zivic, N. Busarsc, S. Milenkovic and N. Grujovic, "General Overview and Applications of Ceramic Matrix Composites (CMCs)," *Encyclopedia of Materials: Composites,* vol. 2, pp. 3-19, 2021.

[15] A. Sathish Marimuthu, C. J. Malathi, V. R. and A. N. Grace, "Processing of ceramics," *Advanced Ceramics for Energy Storage, Thermoelectrics and Photonics,* pp. 19-39, 2023.

[16] B. Clauss, "Fibers for Ceramic Matrix Composites," in *Ceramic Matrix Composites.*, Weinheim, Wiley-VCH Verlag GmbH & Co. KGaA, 2008, pp. pp. 1-20..

[17] A. G. Basukar and A. Kolekar, "A Review on Properties and Applications of Ceramic Matrix Composites," *International Journal of Research in Science and Innovation,* vol. 2, no. Issue XII, pp. 28-30, 2015.

[18] Z. K. Z. L. W. W. L. Y. H. R. Zhang X, "Additive manufacturing of cellular ceramic structures: From structure to structure–function integration," *Materials & Design.,* vol. 215, no. 110470, 2022.

[19] I. Gibson, D. Rosen and B. Stucker, Additive Manufacturing Technologies: 3D Printing, Rapid Prototyping, and Direct Digital Manufacturing, Springer, 2015.

[20] M. H, Y. YK, F. LP, D. KG, Z. H and C. LF., "First 3D printing/molding of carbon fibers reinforced SiOC matrix composites," *Journal of the American Ceramic Society,* vol. 102(10), no. 3244-3255, 2019.

[21] L. Z. L. J. L. C. L. C. F. Y. L. C. L. Y. W. P. H. Y. Chen ZW, "3D printing of ceramics: A review.," *Journal of the European Ceramic Society,* vol. 39(4), pp. 661-687, 2019.

[22] F. C. Z. Q. G.-T. E. D. E. G. F. V. L. S. E. Feilden E, "3D printing bioinspired ceramic composites," *Scientific Reports,* vol. 7, p. 13759, 2017.

[23] A. Zocca, P. Colombo, C. M. Gomes and J. Gunster, "Additive Manufacturing of Ceramics: Issues, Potentialities, and Opportunities," *Journal American Ceramic Society,* p. 19, 2015.

[24] Z. C. Eckel, C. Zhou, J. H. Martin, A. J. Jacobsen, W. B. Carter and T. A. Schaedler, "Additive manufacturing of polymer-derived ceramics," *Science,* no. 351(6268), pp. 58-62, 2016.

[25] J. A. S. J. E. S. J. &. C. J. Lewis, "Direct ink writing of three-dimensional ceramic structures," *Journal of the American Ceramic Society,* no. 89(12), pp. 3599-3609, 2006.

[26] E. Feilden, E. G. T. Blanca, F. Giuliani, E. Saiz and L. J. Vandeperre, "Robocasting of structural ceramic parts with hydrogel inks," *Journal of the European Ceramic Society,* vol. 36(10), pp. 2525-2533, 2016.

[27] F. G., M. H. S., W. L., B. A., P. M. and C. P., "Optimization and characterization of preceramic inks for direct ink writing of ceramic matrix composite structures," *Materials,* vol. Materials, no. 515, 2018.

[28] T. D, W. S. and L. J.A., "Chaotic mixing in three-dimensional microvascular networks fabricated by direct-write assembly," *Nature Materials,* vol. 2, pp. 265-271 , 2003.

[29] G. G. Lewis J.A., "Direct writing in three dimensions," *Materials Today,* vol. 7, pp. 32-39, 2004.

[30] A. B. E. K. M. T. D. Lebel L.L., "Ultraviolet-assisted direct-write fabrication of carbon nanotube/polymer nanocomposite microcoils," *Advanced Materials,* vol. 22, pp. 592-596, 2010.

[31] A. De Marzi, M. Vibrante, M. Botti and G. Franchin, "Development of robot assisted hybrid additive manufacturing technology for the freeform fabrication of lattice structures," *Additive Manufacturing,* pp. 2-3, 2023.

[32] M. Dackweller, S. Countandin and J. Fleischer, "Filament winding for automated joining of lightweight profiles," *JEC Composites Magazine,* vol. 122, pp. 25-26, 2018.

[33] F. Denk, A. Redman, J. Nieschlag, M. Dackweiler, S. Countandin, D. Miller, S. Mecham and T. A. Osswald, "Fabrication of composite truss structures by combination of robotic filament winding and 3D printed adhesive elements," in *CAMX Conference*, Dallas, TX, 2021.

[34] F. R.D., L. L.L. and T. D., "Processing parameters investigation for the fabrication of self-supported and freeform polymeric microstructures using ultraviolet-assisted three-dimensional printing," *Journal of Micromechanics and Microengineering,* vol. 25, no. 055020, 2014.

[35] M. F. Ashby, ""Cellular Solids - Scaling of Properties."," *In Cellular Ceramics: Structure, Manufacturing, Properties and Applications,* pp. 3-17, 2005.

[36] M. Y. T. G. H. S. M. T. E. L. &. K. W. S. Kaur, "3D printed stretching-dominated micro-trusses.," *Materials & Design,* vol. 134, pp. 272-280, 2017.

[37] A. C. P. G. C. M. &. G. J. Zocca, "Additive manufacturing of ceramics: issues, potentialities, and opportunities.," *Journal of the American Ceramic Society,* vol. 98, pp. 1983-2001, 2015.

[38] V. S. F. N. A. &. A. M. F. Deshpande, "Effective properties of the octet-truss lattice material.," *Journal of the Mechanics and Physics of Solids,* vol. 49, pp. 1747-1769, 2001.

[39] C. A. Schneider, W. S. Rasband and K. W. Eliceiri, "NIH Image to ImageJ: 25 years of image analysis," vol. 9, 2012.

[40] L. del-Mazo-Barbara and M.-P. Ginebra, "Rheological characterisation of ceramic inks for 3D direct ink writing: A review," vol. 41, no. 16, 2021.

[41] K. Huang, A. D. Marzi, G. Franchin and P. Colombo, "UV-assisted robotic arm freeforming of SiOC ceramics from a preceramic polymer," *Additive Manufacturing,* vol. 83, no. 104051, p. 10, 2024.

[42] P. Jacobs, "Rapid Prototyping & Manufacturing: Fundamentals of Stereolithography," *Society of Manufacturing Engineers,* 1992.

[43] P. &. B. E. Colombo, "Cellular structures.," *In Ceramics Science and Technology,* pp. 283-311, 2013.

[44] S. B. Nagaraju, H. Priya, Y. G. T. Girijappa and M. Puttegowda, "Lightweight and sustainable materials for aerospace applications," 2023.

[45] H. C. L. &. Z. L. Mei, "Damage mechanisms of C/SiC composites subjected to constant load and oxidative environment.," *Journal of the European Ceramic Society,* vol. 35, pp. 1473-1479, 2015.

[46] H. E. G. F. e. P. C. K. Huang, "Effect of the content and size of PMMA sacrificial particles on the properties of 3D printed polymer-derived SiOC ceramics," *Effect of the content and size of PMMA sacrificial particles on the properties of 3D printed polymer-derived SiOC ceramics,,* vol. 10, no. 2484-2490, 2021.

[47] O. Osuchukwu, A. Salih, I. Abdullahi and .. Obada, "Weibull modulus of a novel mixture of natural hydroxyapatite materials produced from biowastes," *Results in Materials,* vol. 18, no. 100394, 2023.

[48] M. Scheffler and P. Colombo, "Cellular Ceramic Structures: Manufacturing, Properties and Applications," *Advanced Engineering Materials,* vol. 7, no. 1138-1149, 2005.

[50] R. S. Ambeka, B. K. P. Sharma, F. Bosia, M. Fraldi, N. M. Pugno and C. S. Tiwary, "Topologically engineered 3D printed architectures with superior mechanical strength," *materialstoday,* p. 24, 2021.

[51] M. Kaur, T. G. Yun, S. M. Han, E. L. Thomas and W. S. Kim, "3D printed stretching-dominated micro-trusses," *Materials and Design,* p. 11, 2017.

[52] G. &. C. P. Franchin, "Porous geopolymer components through inverse replica of 3D printed sacrificial templates.," *Journal of Ceramic Science and Technology,* vol. 6, pp. 105-112, 2015.

[53] R. Naslain, "Design, preparation and properties of non-oxide CMCs for application in engines and nuclear reactors: an overview.," *Composites Science and Technology,* vol. 64(2), pp. 155-170, 2004.

Ringraziamenti

Un sentito grazie alla mia relatrice Giorgia Franchin e alla mia tutor Anna De Marzi, che hanno sempre visto in me del potenziale e, con i loro preziosi consigli, mi hanno spronata a dare il massimo. La loro fiducia è stata una motivazione fondamentale per la conclusione di questo percorso.

Questa laurea non è solo il frutto del mio impegno, ma anche del supporto che ho ricevuto dalle persone più importanti della mia vita. A voi, dedico con tutto il cuore queste parole di ringraziamento.

Alla mia mamma, che ha reso possibile tutto questo. Sei stata e sei il mio porto sicuro e la mia più grande sostenitrice. Hai fatto sacrifici immensi affinché io potessi studiare e crescere, mi hai insegnato il valore della determinazione e mi hai dato tutto. Grazie per aver sempre creduto in me, anche quando io stessa vacillavo.

A mia sorella, la mia compagna di vita, che ha sempre saputo come risollevarmi nei momenti difficili. Hai sempre la battura pronta per farmi ridere anche quando tutto sembra andare storto e sai come farmi vedere il lato bello delle cose. Grazie per sopportarmi da sempre.

A mia nonna, l'unica che ho, ma che vale per mille. Sei il mio esempio di dolcezza, generosità e amore incondizionato. Ogni tuo gesto, piccolo o grande, ha reso la mia vita più bella e più ricca.

A Giordano, che si prende cura di noi in tanti modi, anche con quei piccoli gesti che fanno la differenza. Grazie di cuore per tutto quello che hai fatto.

Ai ragazzi del gruppo Piston Rangers, che sono diventati molto più di semplici compagni. Abbiamo condiviso fatiche, ore in aula studio, ma anche risate, soddisfazioni e momenti di gioia. Senza di voi, forse avrei mollato perché mi avete fatto capire quanto sia bello avere qualcuno su cui poter contare. Vi sarò sempre grata.

Infine, alle mie amiche di sempre, Gioia e Sara. Siete al mio fianco da quando eravamo bambine, e ancora oggi condividiamo le tappe più importanti delle nostre vite. Sapere che ci siete, sempre e comunque, è un dono prezioso. Grazie per la vostra amicizia e per non avermi mai lasciata sola.

Un grazie di cuore a tutti coloro che, in modi diversi, hanno contribuito al mio benessere durante questo percorso. Agli amici che sono rimasti e a quelli che, pur andandosene, hanno lasciato un segno. A chi ha saputo strapparmi un sorriso nei momenti difficili, essere un confidente nei momenti di bisogno o un supporto. Ognuno di voi ha avuto un ruolo speciale, e ve ne sarò sempre grata.

Ogni contributo, piccolo o grande che sia stato, ha avuto un valore immenso per me. Questa laurea è il "tetto della mia casa", ma è anche il risultato del vostro amore.